JOURNAL OF PETROLOGY | VOLUME 46 | NUMBER 11 | PAGES 2367–2394 | 2005 | doi:10.1093/petrology/egi059

The Geochemistry of Ultramafic to Mafic Volcanics from the Belingwe Greenstone Belt, Zimbabwe: Magmatism in an Archean Continental Large Igneous Province

KENJI SHIMIZU[1]*, EIZO NAKAMURA[1] AND SHIGENORI MARUYAMA[2]

[1]THE PHEASANT MEMORIAL LABORATORY FOR GEOCHEMISTRY AND COSMOCHEMISTRY, INSTITUTE FOR STUDY OF THE EARTH'S INTERIOR, OKAYAMA UNIVERSITY, MISASA, TOTTORI 682-0193, JAPAN

[2]DEPARTMENT OF EARTH AND PLANETARY SCIENCES, TOKYO INSTITUTE OF TECHNOLOGY, TOKYO, 152-8551, JAPAN

RECEIVED APRIL 5, 2004; ACCEPTED MAY 31, 2005
ADVANCE ACCESS PUBLICATION JULY 8, 2005

The evolution of the late Archean Belingwe greenstone belt, Zimbabwe, is discussed in relation to the geochemistry of the ultramafic to mafic volcanic rocks. Four volcanic types (komatiite, komatiitic basalt, D-basalt and E-basalt) are distinguished in the 2·7 Ga Ngezi volcanic sequence using a combination of petrography and geochemistry. The komatiites and D-basalts are rocks in which isotopic systems and trace elements are depleted. Chemical variations in komatiites and D-basalts can be explained by fractional crystallization from the parental komatiite. In contrast, komatiitic basalts and E-basalts are siliceous and display enriched isotopic and trace element compositions. Their chemical trends are best explained by assimilation with fractional crystallization (AFC) from the primary komatiite. AFC calculations indicate that the komatiitic basalts and E-basalts are derived from komatiites contaminated with ~20% and ~30% crustal material, respectively. The volcanic stratigraphy of the Ngezi sequence, which is based on field relationships and the trace element compositions of relict clinopyroxenes, shows that the least contaminated komatiite lies between highly contaminated komatiitic basalt flows, and has limited exposure near the base of the succession. Above these flows, D- and E-basalts alternate. The komatiite appears to have erupted on the surface only in the early stages, when plume activity was high. As activity decreased with time, komatiite magmas may have stagnated to form magma chambers within the continental crust. Subsequent komatiitic magmas underwent fractional crystallization and were contaminated with crust to form D-basalts or E-basalts.

KEY WORDS: *komatiite; crustal assimilation; Belingwe greenstone belt; continental flood basalt; plume magmatism*

INTRODUCTION

Voluminous volcanic rocks were formed worldwide at ~2·7 Ga and provide evidence for intense magmatic activity during this part of the Earth's history. At this time, the growth rate of continental crust may also have been exceptionally high (e.g. Condie, 1998). These events are interpreted to reflect two superimposed processes: (1) the formation of the first supercontinent; (2) enhanced activity in the Earth's mantle (Stein & Hofmann, 1994; Nelson, 1998). To evaluate the magnitude of the 2·7 Ga magmatic activity, it is necessary to constrain the tectonic and chemical evolution of coeval greenstone belts.

A voluminous 2·7 Ga ultramafic to mafic volcanic sequence occurs within the Ngezi Group of the Belingwe greenstone belt, Zimbabwe (Bickle & Nisbet, 1993). The Ngezi Group volcanic sequence is well suited for studying the history of late Archean magmatism because of its excellent preservation and low metamorphic grade. However, most recent geochemical studies have focused only on the fresh komatiites (e.g. Nisbet *et al.*, 1987; McDonough & Ireland, 1993; Shimizu *et al.*, 2001), but not on the voluminous overlying basalts.

*Corresponding author. Telephone: +81-858-43-3828. Fax: +81-858-43-3795. E-mail: shimmy@misasa.okayama-u.ac.jp

Existing data suggest a plume origin for this volcanic sequence (e.g. McDonough & Ireland, 1993; Nisbet *et al.*, 1993*a*). However, controversy exists as to whether the 2·7 Ga Belingwe greenstone belt is autochthonous or allochthonous. Bickle *et al.* (1975, 1994), and, recently, Prendergast (2004) suggested that the Ngezi volcanic sequence was erupted directly onto older continental basement; this appears to be confirmed by the geochemistry of the Belingwe volcanic rocks, which shows evidence of crustal contamination (Chauvel *et al.*, 1993; Bolhar *et al.*, 2003). In contrast, Kusky & Kidd (1992) and Kusky & Winsky (1995) have reported highly strained zones and ultramafic mylonite at the base of the volcanic sequence, which they have interpreted to indicate that an ocean plateau was thrust onto the continent. Sedimentological and structural investigations (Hofmann *et al.*, 2001*a*, 2001*b*) and a geochemical study of shales (Hofmann *et al.*, 2003) have suggested that the sedimentary succession above the Ngezi volcanics formed in a foreland-type sedimentary basin, also implying that the Belingwe greenstone belt is allochthonous. Recently, Shimizu *et al.* (2004) provided direct evidence for an autochthonous continental setting for the Belingwe greenstone belt through the discovery of lower crustal garnet xenocrysts in the komatiites. This discovery also indicates that the Belingwe magmas may have interacted with crustal basement to some extent.

In this paper, we report new geochemical data for 26 least-altered volcanic samples, including komatiite, komatiitic basalt and basalt, and evaluate the geochemical influence of crustal assimilation and fractional crystallization during the transport of magma through the continental crust. We then interpret the evolution of the Ngezi volcanic sequence using the spatial distributions of contaminated and uncontaminated volcanic rocks as determined using trace element analyses (~250 spots on 58 samples) of clinopyroxene relicts.

GEOLOGICAL SETTING

The Belingwe greenstone belt is located in the southern part of Zimbabwe Craton, north of the Limpopo orogenic belt and directly east of the Great Dyke (Fig. 1). It is divided into two groups: the 2·9 Ga lower greenstone belt (Mtshingwe Group) and the 2·7 Ga upper greenstone belt (Ngezi Group). The Belingwe greenstone belt is synformally refolded and cut by several late faults (Kusky & Winsky, 1995). It is bordered on the east and west by ~3·5 and ~2·9 Ga gneissic complexes. The northern and southern borders of the Belingwe greenstone belt are intruded by ~2·6 Ga batholiths (Martin *et al.*, 1993).

The Ngezi Group comprises a very thick (typically 4–6 km) volcanic sequence of ultramafic to mafic lavas (the Reliance and Zeederbergs Formations), which occur between sedimentary units of the Manjeri and Cheshire Formations (e.g. Bickle *et al.*, 1975). The Manjeri Formation is a thin clastic sedimentary succession (maximum thickness 250 m) deposited unconformably on an older felsic basement. The geochemistry of the Manjeri sedimentary rocks indicates that they were derived from a local granitic source (Hunter *et al.*, 1998). The Reliance and Zeederbergs Formations, the focus of this study, consist predominantly of basalt, komatiitic basalt and komatiite, and thin intercalated tuffaceous layers. Chauvel *et al.* (1993) obtained an age of 2692 ± 9 Ma for komatiitic basalts in the Reliance Formation by Pb–Pb dating. The Cheshire Formation, the uppermost stratigraphic unit of the Belingwe greenstone belt, comprises shallow-marine carbonates (Hofmann *et al.*, 2001*b*).

SAMPLE DESCRIPTIONS

The volcanic rocks of this study were sampled to encompass the entire area of the Belingwe greenstone belt (Fig. 1). Although all samples are altered and metamorphosed to some extent, the freshest samples were selected following detailed microscopic observations. Selected samples preserve original textures and igneous relicts of pyroxenes. Hornblende and epidote were not observed, indicating that the metamorphic conditions did not reach the greenschist facies.

Komatiite

Komatiites in the Belingwe greenstone belt are restricted to the Reliance Formation. Selected fresh komatiites were sampled from a single flow unit near the SASKMAR drill site (Nisbet *et al.*, 1987; Renner *et al.*, 1994), the type locality of the Reliance Formation and near the confluence of the main rivers. The ~15 m thick komatiitic flow is composed of a spinifex layer (Fig. 2a) about one-third from top of the flow, a thin B1 layer (~50 cm thick) in the middle and an ~10 m thick cumulate layer (Fig. 2b) at the bottom of the flow. Random and oriented spinifex komatiites occur in the upper and lower part of the spinifex layer, respectively. Cumulate-textured samples contain euhedral olivine and Cr-spinel as cumulate phases and intercumulus acicular clinopyroxene. The acicular clinopyroxene grains have augite cores and, locally, very thin pigeonite rims (<5 μm in width). Secondary serpentine and magnetite occur along cracks and rims of olivine; matrix glass is entirely devitrified. Chlorite is present in the matrix.

Komatiitic basalt

The occurrence of komatiitic basalts is limited to the Reliance Formation. Selected komatiitic basalts were sampled from the type locality of the Reliance Formation and near the confluence of the main rivers, which are close to the Reliance–Zeederbergs Formation boundary.

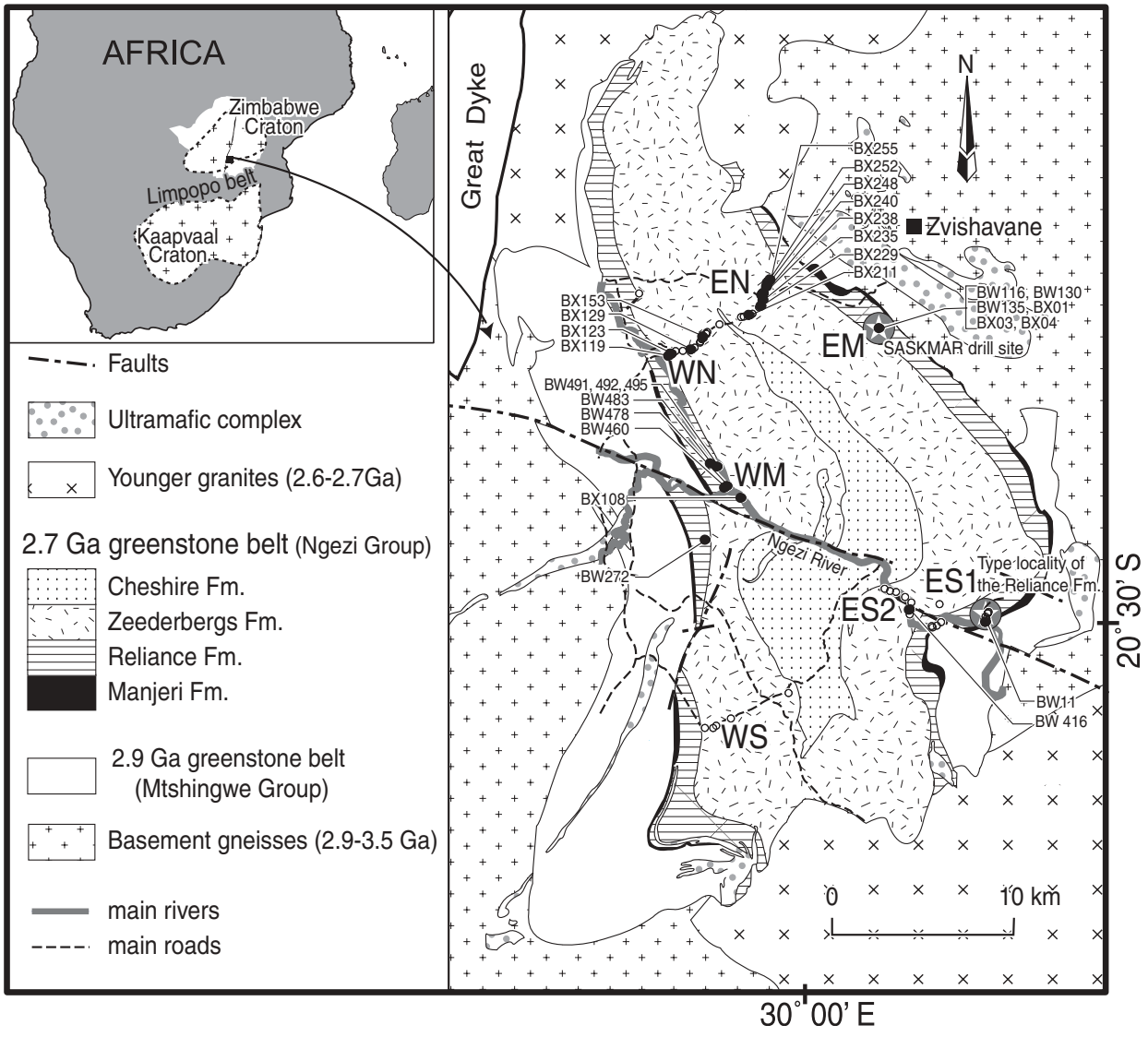

Fig. 1. Geological map of the Belingwe greenstone belt [modified after Nisbet *et al.* (1977)]. Numbered filled and open circles show the localities of samples selected for isotopic analysis of whole rocks or clinopyroxene and for the trace element analysis of clinopyroxene, respectively. The abbreviations E and W refer to the eastern and western parts of the sequence, and N, S and M to the northern, southern and middle parts, respectively.

Komatiitic basalts contain dominantly spinifex-textured pyroxene with minor and small (~20 μm) octahedral Cr-spinel as igneous relict minerals (Fig. 2c). The length and width of the spinifex-textured pyroxenes commonly exceeds 5 mm and 300 μm, respectively. The pyroxenes are composed of a pigeonite core and an augite rim, but pigeonite is mostly replaced by secondary chlorite, calcite and quartz.

Basalt

Pillow and massive basaltic lavas occur throughout the Reliance and Zeederbergs Formations. The least altered basalts were sampled along road cuts for whole-rock analysis. Basalts for clinopyroxene analysis were sampled along the Ngezi River and from the type locality of the Reliance Formation, in addition to road cuts. Most of the basaltic rocks are aphyric with acicular pyroxene (Fig. 2d) and minor groundmass plagioclase, which is mostly replaced by secondary albite. The size of acicular pyroxene grains is up to 100 μm × 500 μm. Chlorite, calcite, pyrite, quartz and albite are present as secondary minerals in the matrix. Quartz and calcite veins are also observed in some basaltic samples. Rare basalts contain euhedral clinopyroxene phenocrysts up to ~500 μm in diameter (Fig. 2e). Ophitic dolerites containing poikilitic clinopyroxene surrounded by unaltered euhedral plagioclase intrude the upper part in the Zeederbergs Formation (Fig. 2f).

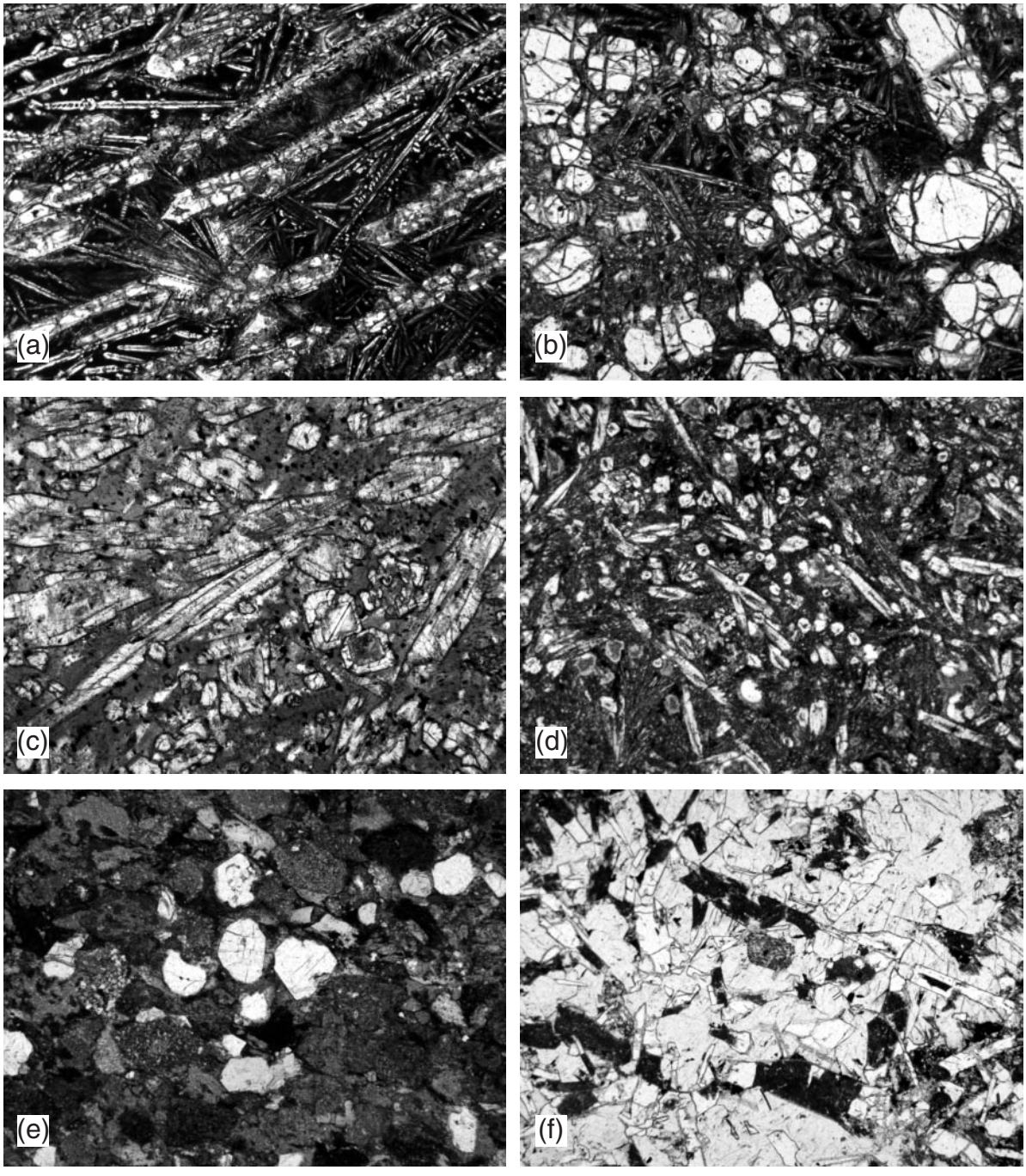

Fig. 2. Photomicrographs of the Belingwe volcanic rocks (field of view 2·5 mm). (a) Spinifex-textured komatiite (BW116) consisting of bladed and oriented olivine with interstitial acicular clinopyroxene. Most of the olivine is replaced by serpentine and chlorite. (b) Ultramafic komatiite in a cumulate layer (BW130) consisting of euhedral olivine phenocrysts and acicular clinopyroxene in a fine-grained groundmass. (c) Komatiitic basalt (BX108) consisting of blocky pyroxenes with pigeonite cores and augite rims. (d) Typical aphyric basalt from the Zeederbergs Formation (BX129) containing acicular clinopyroxene. (e) Metabasalt containing euhedral igneous clinopyroxene phenocrysts (BW416). (f) Ophitic dolerite consisting of poikilitic clinopyroxene surrounding unaltered euhedral plagioclase (Bx153).

ANALYTICAL METHODS

All the analyses were performed at the Pheasant Memorial Laboratory, Institute for Study of the Earth's Interior, Okayama University at Misasa (Nakamura *et al.*, 2003). Rocks were crushed into <5 mm chips using a jaw-crusher, and unaltered pieces were handpicked and washed with deionized water in an ultrasonic bath for 1 h. After drying at 120°C overnight, the chips were

pulverized in an alumina ceramic mill to obtain fine powders with grain size <200 mesh. Major element analyses of whole-rock samples, including Ni and Cr, were determined on fused discs using a Philips PW 2400 X-ray fluorescence spectrometer (Takei, 2002). Loss on ignition (LOI) was determined gravimetrically. Trace element compositions of whole rocks and mineral separates were determined by inductively coupled plasma-mass spectrometry (ICP-MS) using a Yokogawa PMS 2000 system, following the procedures of Makishima & Nakamura (1997) for Li, Rb, Sr, Y, Cs, Ba, REE, Pb, Th and U, Makishima *et al.* (1997) for B, and Makishima *et al.* (1998) for HFSE (high field strength elements; Nb, Zr, Hf and Ta). For Li, Rb, Sr, Y, Cs, Ba, REE, Pb, Th and U abundances and Sr and Nd isotopic ratios, the samples were decomposed with HF–$HClO_4$ in Teflon beakers following the method of Yokoyama *et al.* (1999). Powdered samples for B and HFSE analyses were decomposed with HF in polypropylene bottles. Some studies have found that in ultramafic samples, the HFSE may not be completely recovered using open beaker methods (Tanaka *et al.*, 2003; Blichert-Toft *et al.*, 2004). All komatiite and some basalt samples were, therefore, dissolved at 245°C for 2 days using stainless steel-jacketed Teflon bombs with the aluminum addition method of Tanaka *et al.* (2003) to suppress HFSE coprecipitation with calcium and magnesium fluoride. This set of analyses produced higher Zr and Hf contents (up to 40%) for cumulative komatiites, but similar HFSE contents for basaltic samples. The whole-rock compositions shown in Table 1, except for Rb, Sr, Nd and Sm, are averages of duplicate analyses; the relative differences between replicate analyses were <1% (typically <0·3%) for major element data (but <3% for Cr, Ni, Na, K, P and LOI), and typically <5% for ICP-MS data.

Isotopic ratios of Sr, Nd and Pb and abundances of Rb, Sr, Nd and Sm were determined by thermal ionization mass spectrometry (TIMS), using Finnigan MAT 261 and 262 spectrometers, following the techniques of Yoshikawa & Nakamura (2000) and Kuritani & Nakamura (2002). Mass fractionations during isotopic analysis were corrected by the normalizing factor $^{86}Sr/^{88}Sr = 0{\cdot}1194$ for Sr and $^{146}Nd/^{144}Nd = 0{\cdot}7219$ for Nd and by the 'zero-time correction' method for Pb. The corrected data were normalized using the normalization factors determined from the measured and recommended standard values of NIST SRM 987 ($^{87}Sr/^{86}Sr = 0{\cdot}710240 \pm 19$; Makishima & Masuda, 1994), La Jolla ($^{143}Nd/^{144}Nd = 0{\cdot}511839 \pm 20$; Makishima & Masuda, 1994) and NBS981 ($^{208}Pb/^{204}Pb = 36{\cdot}7266 \pm 42$, $^{207}Pb/^{204}Pb = 15{\cdot}5003 \pm 17$ and $^{206}Pb/^{204}Pb = 16{\cdot}9424 \pm 18$; Kuritani & Nakamura, 2003). The errors on the Pb isotopic ratios are ~0·04% for $^{206}Pb/^{204}Pb$ and $^{207}Pb/^{204}Pb$, and ~0·08% for $^{208}Pb/^{204}Pb$. Although the analytical errors of the Rb, Sr, Sm and Nd abundances are <2% (2σ; $n = 4$), those of the Rb/Sr and Sm/Nd ratios used for the isochrons are remarkably small (~0·3; 2σ % in $n = 4$), because any weighing error, which may be the largest error, cancels out by using a Rb–Sr with Sm–Nd mixed spike. Total procedural blanks for Rb, Sr, Sm, Nd and Pb were less than 5, 25, 0·5, 4 and 50 pg, respectively, and are considered negligible.

Major element compositions of clinopyroxene were determined using a Horiba EMAX-7000 energy dispersive X-ray spectrometer fitted to a Hitachi S-3100H scanning electron microscope at 20 kV accelerating voltage and a sample current of 0·3 nA. Spot size and integral time of each analysis were ~10 μm × 10 μm and 100 s (dead time ~12%). Data were reduced using the standardless ZAF procedure normalized to 100 wt %. Diopside, enstatite and ferrosilite components of pyroxenes are calculated by the method of Lindsley (1983). Spot analyses for trace element compositions of clinopyroxenes were performed using a Cameca ims 5f ion microprobe following the techniques described by Nakamura & Kushiro (1998). Clinopyroxenes from a mantle xenolith were used as standard materials; these standard materials were chemically characterized using ICP-MS. Minerals were sputtered with an O^- primary beam of ~5–15 nA intensity, resulting in a beam size of ~10–15 μm diameter. Positive secondary ions were collected by ion counting using an energy offset of −45 V from 4500 V acceleration with an energy bandpass of ±10 V. The operating conditions resulted in ^{30}Si secondary ion intensities of $(1–1{\cdot}5) \times 10^5$ c.p.s. The secondary ion intensities of the masses concerned were normalized to ^{30}Si. The precision of the data is typically ±5–15%, except for Ba (~30%).

MAJOR AND TRACE ELEMENT COMPOSITIONS

Major and trace element compositions are given in Table 1 and presented in Figs 3 and 4. Loss on ignition for the selected samples is ~4 wt % at most, which is low for Archean greenstones. Even though the selected samples are relatively unaltered, compared with many other Archean volcanic rocks, highly fluid-mobile elements such as K, Li, B, Rb, Cs and Ba are unlikely to preserve original igneous information, because they are not correlated with immobile elements such as Zr.

The negative correlations of MgO with immobile and incompatible elements in the Belingwe komatiites are attributed to fractionation or accumulation of olivine. Although MgO contents range from 16 to 30 wt %, samples with over 25 wt % MgO contain considerable cumulus olivine phenocrysts, often forming as much as ~20 % of the mode (e.g. Bickle *et al.*, 1993). The chemical variations in the Belingwe komatiites are considered to

Table 1: Major and trace element compositions of Belingwe volcanic rocks and igneous relicts

Sample no.:	BW116*	BW130*	BW135*	BW272*	BW460*	BW478*	BW483*	BW491	BW492*	BW495
Rock type:	komatiite	komatiite	komatiite	komatiite	komatiite	komatiite	komatiite	kom basalt	kom basalt	kom basalt
Lithology:	oriented spinifex	cumulate	cumulate	cumulate	cumulate	cumulate	cumulate	pyroxene spinifex	pyroxene spinifex	pyroxene spinifex
Distance:	−530	−540	−540	−340	−320	−160	−240	−110	−110	−110
SiO_2	48·10	45·35	44·86	45·51	44·11	44·60	45·06	53·73	53·55	53·14
TiO_2	0·45	0·30	0·31	0·32	0·25	0·29	0·32	0·53	0·55	0·55
Al_2O_3	8·98	6·08	6·22	6·48	5·06	5·90	6·37	10·84	11·79	11·51
Cr_2O_3	0·23	0·36	0·37	0·36	0·40	0·34	0·36	0·14	0·11	0·11
FeO^T	11·44	10·38	10·42	10·48	10·25	10·19	10·38	9·16	9·37	9·25
MnO	0·20	0·18	0·18	0·18	0·18	0·18	0·18	0·15	0·13	0·14
NiO	0·065	0·18	0·17	0·17	0·22	0·18	0·17	0·024	0·021	0·025
MgO	16·46	27·02	25·42	25·42	30·16	26·99	25·29	10·47	10·55	11·26
CaO	9·02	6·20	6·32	6·60	5·15	6·11	6·57	7·88	7·22	7·16
Na_2O	1·25	0·76	0·60	0·83	0·52	1·01	1·04	3·16	3·06	3·04
K_2O	0·072	0·042	0·061	0·10	0·047	0·078	0·10	0·02	0·03	0·03
P_2O_5	0·033	0·022	0·019	0·022	0·019	0·021	0·023	0·050	0·049	0·051
LOI	2·46	2·15	4·29	2·68	2·75	3·37	2·97	2·92	2·57	2·84
Li	5·4	4·1	5·7	3·4	2·9	4·6	6·7	4·5	4·5	4·3
B	5·3	10	7·1	14	12	4·4	3·3	9·8	5·7	7·7
Rb	1·87	1·00	1·75	1·65	1·30	1·45	1·82	0·369	0·457	0·560
Sr	42·7	29·4	28·4	33·4	24·6	31·6	33·8	48·9	78·5	86·1
Y	10	7·2	7·0	7·3	5·4	6·1	7·0	14	13	13
Zr	19	12	13	13	10	12	12	36	38	33
Nb	0·69	0·46	0·48	0·50	0·38	0·45	0·48	1·5	1·4	1·5
Cs	0·072	0·084	0·11	0·11	0·071	0·050	0·045	0·22	0·24	0·38
Ba	7·7	5·3	4·7	5·8	4·6	8·5	7·2	18	29	34
La	0·91	0·61	0·61	0·52	0·50	0·59	0·58	3·2	3·2	3·1
Ce	2·5	1·8	1·7	1·7	1·4	1·7	1·7	7·4	7·2	7·2
Pr	0·42	0·29	0·29	0·27	0·22	0·28	0·29	1·0	0·96	0·97
Nd	2·46	1·62	1·66	1·67	1·35	1·58	1·68	4·80	4·72	4·47
Sm	0·903	0·595	0·614	0·630	0·494	0·582	0·621	1·42	1·38	1·36
Eu	0·33	0·24	0·24	0·24	0·20	0·24	0·23	0·41	0·48	0·45
Gd	1·2	0·86	0·86	0·83	0·64	0·76	0·85	1·7	1·7	1·7
Tb	0·24	0·17	0·16	0·17	0·13	0·15	0·16	0·33	0·31	0·32
Dy	1·6	1·1	1·1	1·1	0·9	1·0	1·1	2·2	2·0	2·2
Ho	0·35	0·25	0·25	0·25	0·20	0·23	0·24	0·48	0·45	0·47
Er	0·97	0·67	0·69	0·68	0·54	0·62	0·66	1·3	1·2	1·3
Tm	0·15	0·11	0·10	0·11	0·08	0·09	0·11	0·21	0·19	0·20
Yb	1·0	0·74	0·75	0·74	0·58	0·68	0·71	1·4	1·3	1·4
Lu	0·15	0·11	0·11	0·11	0·08	0·10	0·11	0·20	0·19	0·20
Hf	0·59	0·39	0·39	0·39	0·32	0·37	0·39	1·02	1·1	0·97
Ta	0·047	0·033	0·033	0·032	0·028	0·031	0·031	0·104	0·12	0·11
Pb	0·20	0·13	0·11	0·09	0·12	0·12	0·10	0·91	0·70	1·2
Th	0·094	0·064	0·061	0·048	0·058	0·066	0·060	0·98	0·91	1·0
U	0·032	0·022	0·021	0·017	0·019	0·022	0·020	0·32	0·30	0·34

result from redistribution of olivine crystals during emplacement of komatiitic flows at the surface (Renner *et al.*, 1994; Silva *et al.*, 1997). Thus, the undifferentiated (primary) composition of the komatiitic magma lies between spinifex komatiite and cumulate (e.g. Arndt, 1994; Renner *et al.*, 1994). The komatiites are slightly depleted in light rare earth elements [LREE; Fig. 4, $(La/Sm)_N$ 0·6–0·7, where N denotes chondrite

Sample no.:	BX001*	BX003*	BX004*	BX108	BX119	BX123	BX129	BX153	BX211*	BX229
Rock type:	komatiite	komatiite	komatiite	kom basalt	basalt	basalt	basalt	basalt	basalt	basalt
Lithology:	random spinifex	B1 layer	B1 layer	pyroxene spinifex	pillow lava	massive lava	massive lava	massive lava	pillow lava	pillow lava
Distance:	−530	−530	−530	−110	450	600	1630	2560	2740	1930
SiO_2	46·00	47·80	47·70	51·04	51·80	52·36	53·21	50·25	52·59	52·17
TiO_2	0·34	0·43	0·43	0·55	0·56	0·55	0·53	1·25	0·62	0·53
Al_2O_3	6·88	8·72	8·73	11·27	13·81	13·21	13·30	13·79	14·33	12·97
Cr_2O_3	0·45	0·36	0·35	0·14	0·050	0·049	0·051	0·026	0·036	0·07
FeO^T	10·70	11·31	11·25	9·95	9·28	9·42	9·04	11·82	9·82	7·93
MnO	0·18	0·20	0·20	0·18	0·16	0·18	0·16	0·26	0·19	0·17
NiO	0·15	0·075	0·074	0·026	0·019	0·017	0·013	0·014	0·011	0·022
MgO	24·02	17·07	16·90	11·48	8·26	8·01	8·59	6·20	7·52	9·72
CaO	6·94	8·94	8·89	8·54	10·85	10·78	8·96	10·85	6·58	10·29
Na_2O	0·80	1·22	1·24	2·84	1·68	2·24	1·86	1·68	2·18	1·57
K_2O	0·058	0·078	0·085	0·023	0·088	0·035	0·080	0·10	1·73	0·01
P_2O_5	0·025	0·030	0·030	0·051	0·044	0·043	0·054	0·11	0·069	0·054
LOI	2·41	2·41	2·93	2·59	2·32	2·18	3·33	2·20	3·17	3·93
Li	3·2	7·5	8·1	2·7	6·9	5·2	8·5	7·9	9·0	3·9
B	2·9	3·6	3·6	5·5	14	15	11	8·1	15	21
Rb	1·23	1·30	1·52	0·791	2·46	0·460	2·52	2·25	57·83	0·140
Sr	32·7	43·0	42·6	108	144	112	165	91·0	79·3	32·4
Y	8·0	10	10	13	12	13	15	30	21	15
Zr	14	18	19	34	23	23	30	66	52	30
Nb	0·51	0·63	0·67	1·4	0·93	1·01	1·3	2·9	1·9	0·92
Cs	0·041	0·049	0·053	0·17	0·23	0·28	0·31	0·12	0·55	0·10
Ba	4·5	9·2	9·6	20	20	46	20	29	597	20
La	0·66	0·92	0·90	3·0	1·2	1·3	3·2	3·5	5·6	2·4
Ce	1·9	2·6	2·6	7·0	3·6	3·7	7·1	10	12	5·3
Pr	0·32	0·43	0·43	0·93	0·57	0·60	0·90	1·6	1·5	0·70
Nd	1·84	2·36	2·36	4·45	3·12	3·21	4·15	8·19	6·50	3·44
Sm	0·675	0·867	0·867	1·33	1·08	1·13	1·28	2·68	1·84	1·16
Eu	0·26	0·36	0·35	0·50	0·49	0·45	0·56	1·04	0·61	0·58
Gd	0·92	1·3	1·2	1·7	1·5	1·6	1·8	3·7	2·4	1·7
Tb	0·18	0·25	0·25	0·32	0·29	0·30	0·35	0·70	0·45	0·33
Dy	1·2	1·6	1·6	2·1	1·9	2·1	2·5	4·7	3·1	2·3
Ho	0·28	0·38	0·37	0·47	0·44	0·47	0·55	1·0	0·70	0·54
Er	0·76	1·0	0·99	1·3	1·2	1·3	1·5	2·9	1·9	1·5
Tm	0·12	0·16	0·16	0·21	0·19	0·20	0·24	0·44	0·30	0·24
Yb	0·80	1·1	1·1	1·4	1·3	1·4	1·7	3·1	2·1	1·6
Lu	0·12	0·16	0·16	0·20	0·19	0·21	0·25	0·45	0·31	0·24
Hf	0·44	0·54	0·59	1·00	0·73	0·75	0·97	1·9	1·5	0·97
Ta	0·036	0·042	0·044	0·10	0·062	0·065	0·10	0·19	0·15	0·071
Pb	0·23	0·23	0·22	1·2	0·19	0·18	1·4	0·51	2·1	1·1
Th	0·077	0·11	0·10	0·98	0·13	0·13	1·1	0·31	1·9	0·74
U	0·026	0·036	0·036	0·33	0·044	0·044	0·33	0·09	0·60	0·22

normalized value; McDonough & Sun, 1995] similar to previously published data (e.g. Bickle *et al.*, 1993).

The chemical compositions of the komatiitic basalts are relatively constant, which is probably due to sampling at the same location. Those komatiitic basalts that have high MgO (~11 wt %) and SiO_2 (~54 wt %) contents fall into the compositional field of siliceous high-magnesium basalts (SHMB) observed in other Archean

Table 1: continued

Sample no.:	BX235	BX238	BX240	BX248	BX252	BX255	BW11px	BW416 px	BW492 px	BX153pl	JB-3
Rock type:	basalt	basalt	basalt	basalt	basalt	basalt	basalt	basalt	kom basalt	basalt	basalt
Lithology:	pillow lava	pillow lava	pillow lava	pillow lava	pillow lava	pillow lava	clino-pyroxene	clino-pyroxene	clino-pyroxene	plagio-clase	GSJ standard
Distance:	1670	1500	1450	1120	950	760	−1200	680	−110	2560	
SiO_2	52·19	48·12	47·73	48·72	48·56	48·50					
TiO_2	0·53	0·73	0·75	0·73	0·74	0·74					
Al_2O_3	14·24	14·16	14·67	14·26	14·48	14·52					
Cr_2O_3	0·060	0·055	0·057	0·055	0·057	0·061					
FeO^T	8·29	10·96	11·09	10·90	10·99	10·73					
MnO	0·14	0·19	0·19	0·19	0·19	0·18					
NiO	0·015	0·023	0·023	0·023	0·023	0·025					
MgO	9·00	8·28	8·43	7·48	8·36	8·42					
CaO	7·51	11·91	11·73	13·46	11·66	11·98					
Na_2O	3·95	1·83	1·28	0·82	1·67	1·16					
K_2O	0·015	0·062	0·15	0·093	0·046	0·18					
P_2O_5	0·049	0·059	0·064	0·059	0·059	0·059					
LOI	3·36	2·55	2·64	2·30	2·07	2·41					
Li	4·8	6·4	8·7	5·8	5·7	7·4					7·29
B	10	13	7·8	9·2	7·4	8·4					20·9
Rb	0·185	1·13	4·57	2·77	0·911	7·59	0·0722	0·0226	0·0220	1·48	15·4
Sr	60·1	202	114	209	141	163	5·17	33·7	5·07	182	423
Y	16	18	19	18	18	17	11	5·1	14	0·79	28·6
Zr	24	32	35	35	33	31					87·9
Nb	0·90	1·4	1·5	1·4	1·6	1·5					1·89
Cs	0·33	0·14	0·19	0·050	0·11	0·12	0·007	0·001	0·001	0·025	0·95
Ba	24	26	33	18	18	30	2·4	0·3	0·2	19	240
La	2·2	2·0	2·1	1·9	2·0	1·9	0·17	0·56	0·43	0·25	8·36
Ce	5·1	5·6	5·9	5·5	5·6	5·5	0·7	2·0	1·6	0·6	21·6
Pr	0·68	0·87	0·94	0·84	0·92	0·84	0·18	0·42	0·29	0·10	3·23
Nd	3·34	4·60	4·83	4·62	4·85	4·69	1·28	2·68	2·13	0·428	16·1
Sm	1·17	1·58	1·64	1·57	1·65	1·61	0·711	0·966	1·00	0·115	4·23
Eu	0·49	0·61	0·68	0·66	0·73	0·65	0·31	0·42	0·36	0·28	1·35
Gd	1·7	2·2	2·3	2·1	2·3	2·1	1·2	1·1	1·7	0·13	4·53
Tb	0·35	0·42	0·44	0·41	0·44	0·41	0·26	0·18	0·36	0·026	0·76
Dy	2·5	2·9	2·9	2·8	2·9	2·8	1·9	1·1	2·5	0·16	4·65
Ho	0·56	0·64	0·65	0·61	0·65	0·63	0·42	0·20	0·55	0·03	0·98
Er	1·5	1·8	1·8	1·7	1·8	1·7	1·1	0·45	1·5	0·07	2·58
Tm	0·25	0·27	0·28	0·26	0·28	0·27	0·17	0·07	0·23	0·01	0·39
Yb	1·7	1·9	2·0	1·9	2·0	1·8	1·2	0·40	1·6	0·08	2·67
Lu	0·25	0·28	0·29	0·27	0·28	0·26	0·17	0·056	0·23	0·010	0·38
Hf	0·82	1·00	1·1	1·1	1·0	1·0					2·63
Ta	0·064	0·089	0·10	0·09	0·10	0·094					0·118
Pb	1·2	0·59	0·37	0·69	0·44	0·38	0·12	0·10	0·10	0·13	5·09
Th	0·64	0·18	0·18	0·17	0·18	0·16	0·0085	0·0070	0·050	0·012	1·27
U	0·19	0·054	0·053	0·053	0·055	0·052	0·0034	0·0038	0·0089	0·0036	0·48

Distance (in m) indicates the sampling positions which are measured vertically from the boundary between the Reliance and Zeederbergs Formations without considering the dips of the lavas. Samples from the Reliance and Zeederbergs Formations are shown by negative and positive values of distance, respectively. LOI, loss on ignition. SiO_2 to LOI in wt %; Li to U in ppm. JB-3 is standard rock sample used as an internal standard for ICP-MS analyses. Kom, komatiitic.
*For Zr, Nb, Hf and Ta abundances, samples were decomposed using a Teflon bomb with the Al-addition method of Tanaka *et al*. (2003).

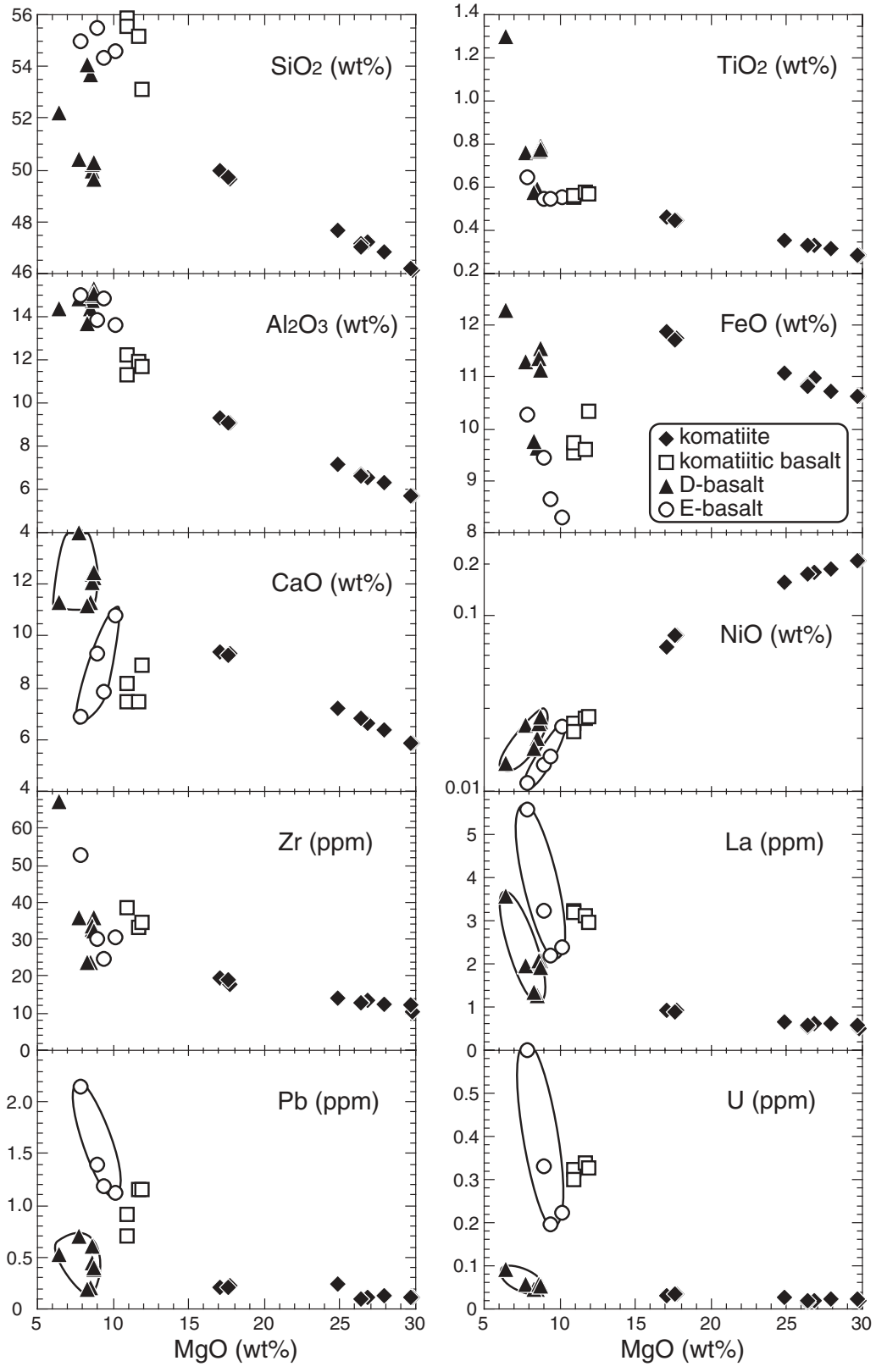

Fig. 3. Major and trace element variations vs MgO (wt %) in the Belingwe volcanic rocks. Basaltic rocks are classified into two types (D- and E-basalt) based on their CaO, NiO, La, Pb and U contents.

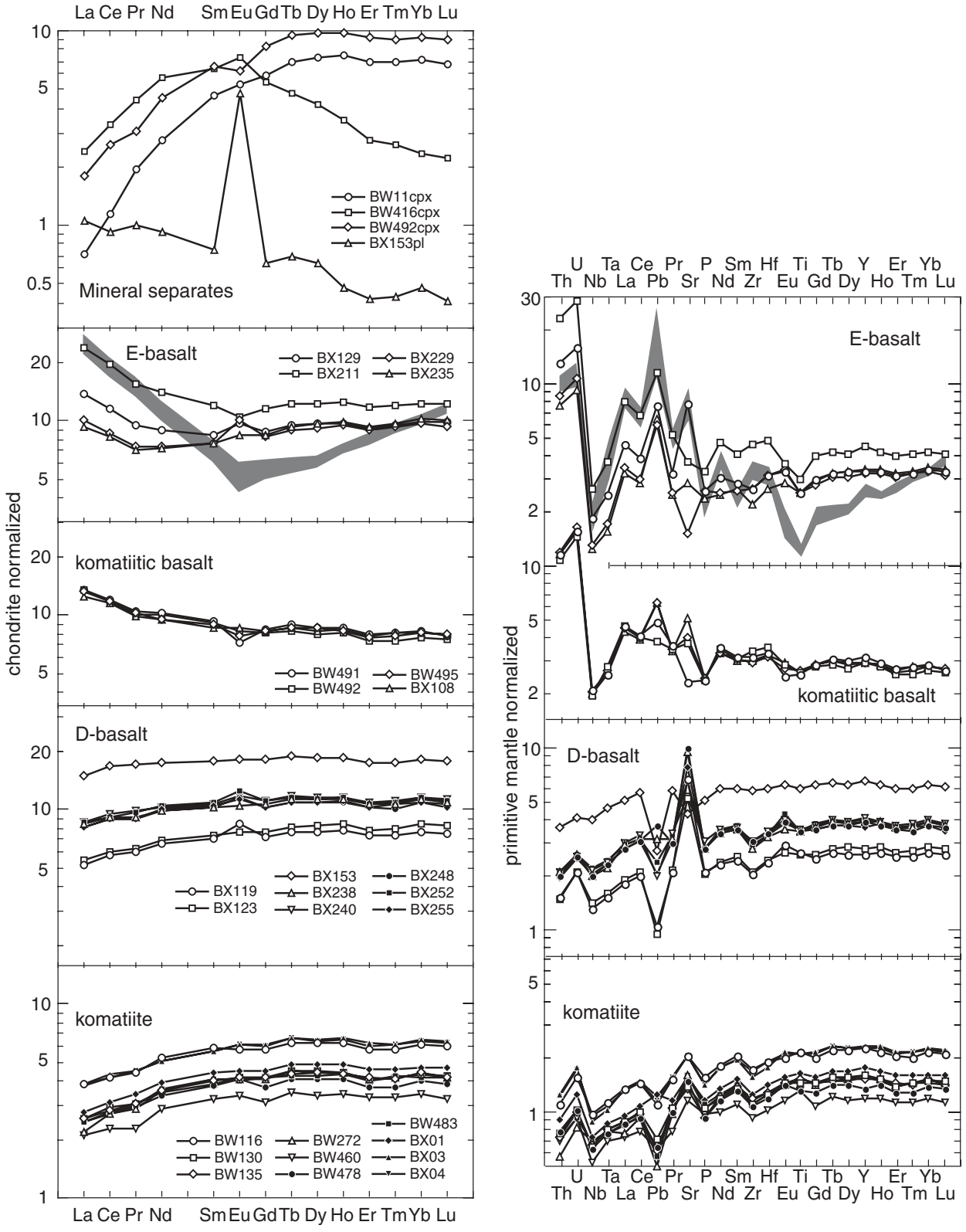

Fig. 4. Rare earth element patterns of whole rocks and mineral separates (pl, plagioclase; cpx, clinopyroxene) normalized to the chondrite values of McDonough & Sun (1995); trace element patterns of whole rocks normalized to the primitive mantle values of McDonough & Sun (1995). Gray fields in the E-basalt diagrams show the compositional ranges of 10 boninite-like rocks from Smithies (2002) and Smithies *et al.* (2004).

greenstone belts (e.g. Redman & Keays, 1985; Arndt & Jenner, 1986). The Belingwe komatiitic basalts have low abundances of CaO and FeO, and enrichment of Zr, La, Pb and U (Fig. 3), which cannot be simply explained by fractionation of olivine from the komatiites. The highly enriched LREE patterns of the komatiitic basalts [Fig. 4; $(La/Sm)_N$ 1·5] also indicate that they were not derived from the komatiites by fractional crystallization.

The basalts exhibit a small range in MgO contents, from 6 to 9 wt %, but with large ranges of elements such as SiO_2, FeO and CaO. Although the basalts can be clearly divided into two types by their chemical compositions, especially by REE patterns (Fig. 4), these are not obviously different petrographically. LREE-depleted [$(La/Sm)_N$ 0·7–0·8] and -enriched [$(La/Sm)_N$ 1·2–2·0] basalts are defined as D-basalts and E-basalts, respectively. Apart from LREE depletion, D-basalts also tend to have higher CaO, FeO, NiO and TiO_2 contents and lower SiO_2, La, Pb and U contents than E-basalts (Fig. 3). E-basalts also display slightly U-shaped REE profiles [$(Yb/Gd)_N \sim 0{\cdot}9$] that resemble those of Phanerozoic boninites. Two samples of D-basalt (BX119 and BX123) have higher SiO_2 and lower REE contents than other D-basalts, but display similar patterns to other D-basalts.

ISOTOPIC COMPOSITIONS

Isotope data obtained from the Belingwe volcanic rocks are presented in Table 2 and the isotopic variation diagrams are shown in Figs 5–7.

Pb–Pb ages of the komatiitic basalt and E-basalt are 2655 ± 88 Ma and 2660 ± 33 Ma, respectively, which are identical within error to the Pb–Pb ages reported by Chauvel *et al.* (1993). μ1 values (apparent μ values: $^{238}U/^{204}Pb$ calculated using the isochrons and an age of 4550 Ma for the formation of the Earth) for komatiitic basalts and E-basalts are clearly different from one another. Although the isochrons for komatiite and D-basalt have a large uncertainty, they are parallel to those of komatiitic basalt and E-basalt. μ1 values of komatiite and D-basalt are not clearly different, but are lower than those of komatiitic basalt and E-basalt.

The Sm–Nd isochron age for the Belingwe volcanics obtained by Chauvel *et al.* (1993) was imprecise because of the small variations of Sm/Nd ratios in the whole rocks. In this study, we obtained more precise Sm–Nd ages for the Belingwe volcanic rocks by broadening the range of Sm/Nd ratios by analyzing igneous relict minerals (Fig. 6). Two clear isochrons were obtained, and the resultant Sm–Nd ages for the D-basalt and komatiitic basalt are 2698 ± 82 Ma and 2672 ± 64 Ma, respectively. These are identical within error to the Pb–Pb ages. Thus, our data support an age of 2·7 Ga for the Ngezi Group, as reported by Chauvel *et al.* (1993). As the komatiites have a small range of Sm/Nd ratios, their isochron age is uncertain. E-basalts show a wider spread in Sm/Nd ratios, but their age has a large error. The total range of εNd (2·7 Ga) values for all the volcanic rock types is from −0·4 to +2·1, as shown in Table 2.

Whole-rock Rb–Sr isochrons for the Belingwe volcanics (Fig. 8) are unlikely to be reliable, because these elements are highly mobile during alteration. However, the Sr isotopic compositions of igneous relict minerals may preserve their original igneous features, as suggested by Machado *et al.* (1986). Initial Sr isotopic ratios of clinopyroxene were calculated based on an age of 2·7 Ga and their measured Rb/Sr ratios (Table 2). Although the plagioclase is igneous, the impurity of plagioclase mineral separates because of the presence of secondary albite may have caused an increase in Rb content and consequently a decrease in the initial $^{87}Sr/^{86}Sr$ ratios. Thus, the initial $^{87}Sr/^{86}Sr$ ratio for the D-basalts is determined to be 0·7010 from the clinopyroxene, which is identical to that of igneous relict minerals from the 2·7 Ga Abitibi greenstone belt within error (Machado *et al.*, 1986). Those for komatiitic basalt and E-basalt are slightly more radiogenic at 0·7015.

CLINOPYROXENE COMPOSITIONS

Clinopyroxene compositions from the Belingwe volcanic rocks are presented in Table 3. Analyzed clinopyroxenes are of variable size (∼20–500 μm) and texture (skeletal, acicular, subhedral or euhedral). The textures indicate that most of them crystallized rapidly after eruption of the magma at the surface. The Mg-number of augite in the komatiites decreases with decreasing wollastonite content from core to rim; the outermost-rim pigeonites have substantially lower Mg-numbers (Fig. 8). In the komatiitic basalts, the pigeonite cores have relatively high Mg-number and augite mantles have lower Mg-number (Fig. 8). The difference in the crystallization sequence of the pyroxenes between komatiite (augite < pigeonite) and komatiitic basalt (pigeonite < augite) is attributed to the different major element compositions of the magmas. For the komatiite, olivine crystallizes as the liquidus phase, and the residual liquid moves away from the projection of the bulk composition of komatiite toward the olivine–augite cotectic curve, as shown in the phase diagram of Kinzler & Grove (1985; Fig. 9). When the liquid reaches this curve, augite joins the crystallization assemblage and the liquid follows the curve to the reaction point, where pigeonite appears. For the komatiitic basalt, after olivine crystallization, the liquid reaches the olivine–pigeonite reaction curve and follows this curve by reacting olivine and liquid, resulting in crystallization of pigeonite until the liquid reaches the reaction point where augite joins the crystallization assemblage (Fig. 9). In basaltic samples, pigeonite is very rare. Augite in the D-basalts tends to

Table 2: Pb, Nd and Sr isotopic compositions for the Belingwe volcanic rocks and igneous relicts

Sample	$^{206}Pb/^{204}Pb$	$^{207}Pb/^{204}Pb$	$^{208}Pb/^{204}Pb$	μ1	$^{147}Sm/^{144}Nd$	$^{143}Nd/^{144}Nd$	εNd (2·7 Ga)	$^{87}Rb/^{86}Sr$	$^{87}Sr/^{86}Sr$	$^{87}Sr/^{86}Sr_{Int}$ (2·7 Ga)
Komatiite										
BW116	18·08	15·49	36·93	8·1	0·222	0·513196 ± 6	2·1	0·127	0·706773 ± 8	
BW130	18·09	15·56	37·10		0·222	0·513236 ± 7		0·0982	0·704774 ± 9	
BW135					0·224	0·513234 ± 6		0·179	0·709972 ± 8	
BW272	18·65	15·56	37·36		0·228	0·513296 ± 6		0·143	0·707813 ± 8	
BW460	18·10	15·54	37·15		0·222	0·513188 ± 5		0·153	0·708557 ± 7	
BW478	18·63	15·63	37·55		0·222	0·513188 ± 5		0·133	0·707448 ± 9	
BW483					0·223	0·513216 ± 7		0·156	0·707152 ± 8	
BX01	17·48	15·45	36·62		0·222	0·513183 ± 6		0·109	0·705245 ± 8	
BX03	18·41	15·63	37·42		0·222	0·513204 ± 6		0·0874	0·704409 ± 9	
BX04	18·48	15·64	37·48		0·222	0·513183 ± 6		0·103	0·705077 ± 7	
D-basalt										
BX119	20·18	15·79	38·84	8·0	0·209	0·512964 ± 7	1·7	0·0493	0·702875 ± 8	
BX123	21·52	16·06	39·98		0·213	0·512995 ± 7		0·0119	0·702836 ± 9	
BX153	18·07	15·33	37·81		0·198	0·512751 ± 5		0·0717	0·703599 ± 8	
BX238	16·42	15·20	35·98		0·207	0·512880 ± 6		0·0162	0·702689 ± 8	
BX240	18·10	15·42	37·56		0·206	0·512884 ± 6		0·116	0·705937 ± 8	
BX248	15·90	15·19	35·40		0·206	0·512881 ± 7		0·0384	0·703060 ± 8	
BX252	17·37	15·37	36·84		0·206	0·512846 ± 5		0·0187	0·701912 ± 9	
BX255	17·02	15·30	36·43		0·207	0·512917 ± 8		0·134	0·706126 ± 8	
BW11px					0·337	0·515237 ± 6		0·0404	0·702621 ± 11	0·7010
BX153pl					0·163	0·512182 ± 15		0·0236	0·701359 ± 8	0·7004
Komatiitic basalt										
BW491	24·84	16·90	42·90	8·4	0·179	0·512350 ± 9	0·7	0·0219	0·705314 ± 8	
BW492	27·07	17·30	44·47		0·177	0·512317 ± 5		0·0168	0·703080 ± 7	
BW495	21·69	16·32	40·19		0·183	0·512427 ± 7		0·0188	0·704496 ± 9	
BX108	22·53	16·49	40·85		0·180	0·512389 ± 7		0·0211	0·702801 ± 7	
BW492px					0·284	0·514208 ± 4		0·0125	0·701929 ± 9	0·7014
E-basalt										
BX129	22·13	16·65	41·33	9·0	0·187	0·512493 ± 6	−0·35	0·0442	0·703872 ± 8	
BW211	23·60	16·86	42·86		0·171	0·512149 ± 5		2·12	0·770418 ± 9	
BX229	20·54	16·36	39·94		0·205	0·512756 ± 6		0·0125	0·704055 ± 8	
BX235	19·91	16·25	39·38		0·213	0·512918 ± 5		0·00890	0·705598 ± 8	
BW416px					0·218	0·513053 ± 3	0·6	0·00193	0·701622 ± 10	0·7015

Analytical precision for isotope data of Nd and Sr are 2σ mean. μ1 indicates apparent μ values calculated using isochrons for samples of each rock type and an age of 4·55 Ga for the Earth. εNd displays deviation in parts per 10^4 from the chondritic reference reservoir at 2·7 Ga. The errors of εNd and $^{87}Sr/^{86}Sr_{Int}$ considering the analytical uncertaintities are ∼0·5 and negligible, respectively. $^{87}Sr/^{86}Sr_{Int}$ values of whole rocks are not shown because they may have changed during alteration.

have slightly higher wollastonite contents and lower Mg-number than that in the E-basalts (Fig. 8). Compositional ranges of augite in the Belingwe komatiites overlap those in Barberton komatiites of Parman *et al.* (1997), but with slightly higher wollastonite contents and lower Mg-number. Although Parman *et al.* (1997) suggested that the high wollastonite contents of augite in komatiites indicate crystallization from a water-saturated magma at 2 kbar, augite with higher wollastonite contents from the Belingwe komatiite clearly did not crystallize at such high pressure, and thus may not have formed from a water-rich magma.

The REE patterns of augite in the volcanic rocks are different in each magma type (Fig. 10). Trace element

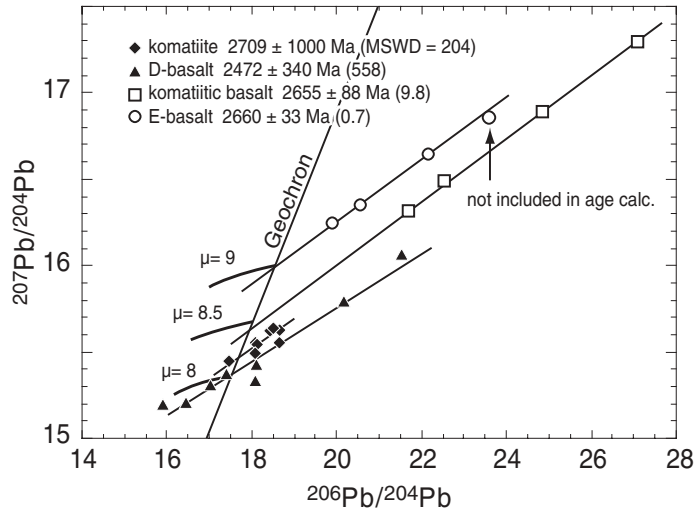

Fig. 5. $^{207}Pb/^{204}Pb$ vs $^{206}Pb/^{204}Pb$ isochron diagram for the whole rocks, showing four parallel isochrons. One E-basalt (BX211) with 1·7 wt % K_2O is not included in the age calculations because it may have suffered substantial low-temperature alteration. The ages and mean square weighted deviations (MSWD) of the isochrons for each rock type are shown in the legend. Geochron and the curves for μ of 8, 8·5 and 9 are plotted following calculations and parameters of Faure (1986).

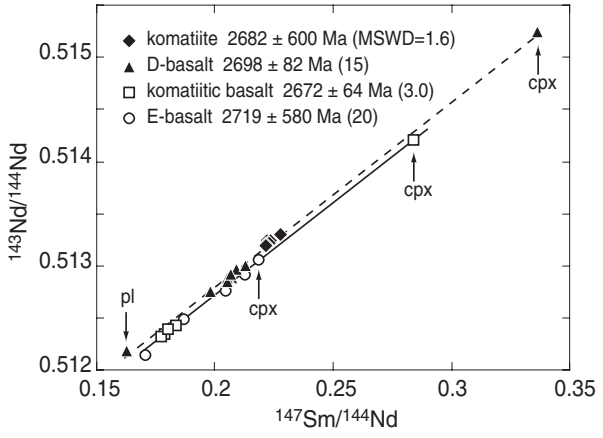

Fig. 6. $^{143}Nd/^{144}Nd$ vs $^{147}Sm/^{144}Nd$ diagram for whole rocks and igneous clinopyroxene (cpx) and plagioclase (pl) relicts. The continuous line and the dashed line are isochrons for komatiitic basalt and D-basalt, respectively. The ages and mean square weighted deviations (MSWD) of the isochrons for each rock type are shown in the legend. The clinopyroxene of the E-basalt is not included in the age calculation.

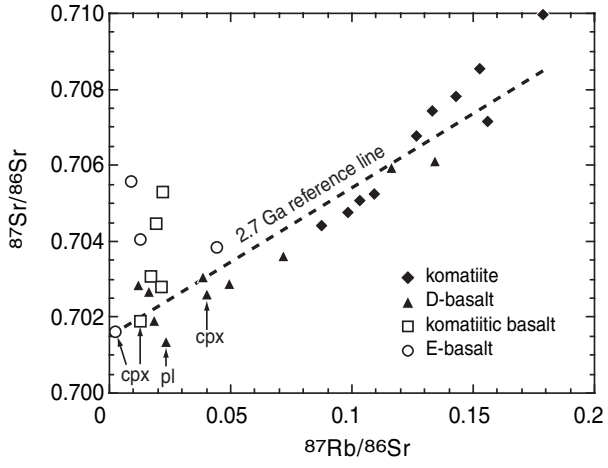

Fig. 7. $^{87}Sr/^{86}Sr$ vs $^{87}Rb/^{86}Sr$ diagram for whole rocks and igneous clinopyroxene (cpx) and plagioclase (pl) relicts. The dashed line indicates a 2·7 Ga reference isochron.

compositions of augite in equilibrium with the lavas were calculated using the respective whole-rock compositions and the clinopyroxene–melt partition coefficients (*D*) of Hart & Dunn (1993), following the approach of Parman *et al.* (2003). We have not corrected the calculated melt compositions for mineral abundances in the samples, because olivine and spinel (which were the dominant phrases to accumulate or crystallize in these samples) have low REE concentrations. This simplification does not affect the relative concentrations of REE. Augite trace element compositions calculated from the whole-rock compositions of the samples display similar patterns to those measured in relict augite in the rocks of each magma type (Fig. 10). However, the calculated concentrations are overall lower than the measured ones because we have not corrected for the effects of the olivine and spinel fractionation.

DISCUSSION ON THE CHEMICAL VARIATIONS OF THE VOLCANICS

To simulate the whole-rock compositional variation of volcanic rocks from the 2·7 Ga Belingwe greenstone belt, an assimilation–fractional crystallization (AFC) calculation was performed for both major and trace element compositions (see the Appendix for a detailed explanation). First, the composition of the parental komatiite was

Table 3: Major and trace element compositions of selected clinopyroxene in the Belingwe volcanics

Sample no.:	BW008	BW011	BW033	BW050	BW052	BW069	BW072	BW087	BW091	BW214	BW242	BW250	BW337	BW357	BW395
Lithology:	basalt	basalt	basalt	Kbasalt	Kbasalt	komatiite	komatiite	komatiite	komatiite	basalt	basalt	basalt	basalt	basalt	basalt
Texture:	subhedral	euhedral	spinifex	spinifex	spinifex	spinifex	spinifex	spinifex	spinifex	spinifex	euhedral	euhedral	euhedral	euhedral	euhedral
Locality:	ES1	ES1	ES1	ES1	ES1	ES1	ES1	ES1	ES1	WS	WS	WS	ES1	ES2	WN
Distance:	−1230	−1200	−1060	−920	−920	−820	−820	−760	−800	5220	1750	860	620	−840	10
SiO_2	53·6	53·6	54·3	53·3	54·1	52·5	52·7	52·2	52·3	51·7	53·4	53·6	54·1	53·3	53·9
TiO_2	0·3	0·2	0·1	0·3	0·1	0·3	0·3	0·4	0·4	0·6	0·3	0·3	0·1	0·3	0·2
Al_2O_3	1·8	3·3	1·9	3·4	3·1	4·7	4·6	5·0	4·6	5·7	2·9	2·2	2·9	2·0	2·7
Cr_2O_3	0·0	0·3	0·1	0·2	0·3	0·4	0·1	0·2	0·2	0·2	0·3	0·0	0·5	0·0	0·2
FeO	10·9	5·0	8·3	6·9	6·6	5·7	7·6	5·2	7·0	6·5	7·4	9·4	6·5	10·8	7·0
MnO	0·3	0·1	0·2	0·2	0·1	0·2	0·1	0·2	0·2	0·2	0·2	0·1	0·1	0·3	0·1
MgO	15·0	17·2	17·4	18·0	18·9	16·1	17·7	16·3	17·6	16·6	17·2	16·4	18·4	15·1	17·7
CaO	17·9	20·2	17·4	17·5	16·6	19·8	16·7	20·1	17·4	18·3	18·0	17·7	17·1	17·6	17·9
Na_2O	0·3	0·2	0·2	0·1	0·2	0·3	0·2	0·2	0·3	0·3	0·2	0·3	0·2	0·5	0·3
Sr	9·0	5·4	6·6	6·4	6·1	8·1	7·1	6·9	8·1	5·9	5·9	7·3	5·5	6·3	5·0
Y	33	7·5	8·0	13	11	13	16	12	16	23	13	15	9·3	10	10
Zr	15	4·8	2·6	10	8·1	13	14	13	13	32	7·3	5·5	5·2	5·0	4·0
Nb	0·002	0·006	0·002	0·006	0·010	0·015	0·004	0·007	0·006	0·008	0·007	0·001	0·011	0·001	0·004
Ba	0·3	0·1	0·1	0·2	0·0	0·1	0·2	0·1	0·2	0·3	0·0	0·0	0·0	0·3	0·0
La	0·3	0·1	0·1	0·3	0·2	0·2	0·2	0·2	0·3	0·6	0·1	0·2	0·5	0·2	0·1
Ce	2·2	0·5	0·5	1·1	0·8	0·9	0·8	0·9	1·2	2·4	0·7	0·8	1·7	0·7	0·5
Pr	0·5	0·1	0·1	0·2	0·2	0·2	0·2	0·2	0·3	0·5	0·2	0·2	0·3	0·1	0·1
Nd	3·9	0·8	0·8	1·5	1·5	1·5	1·9	1·3	2·2	3·1	1·6	1·5	2·1	1·3	1·0
Sm	2·8	0·4	0·4	0·7	0·6	1·3	1·2	0·8	1·1	1·5	0·7	0·8	0·8	0·7	0·7
Eu	0·9	0·1	0·2	0·3	0·3	0·4	0·4	0·3	0·4	0·5	0·2	0·4	0·2	0·3	0·2
Gd	3·1	0·7	0·8	1·8	1·6	1·8	1·8	1·4	1·8	2·2	1·4	1·5	1·3	1·2	1·2
Dy	5·9	1·2	1·2	2·2	1·7	2·7	2·9	1·8	2·5	3·9	1·9	2·3	1·5	1·7	1·5
Er	3·2	0·8	0·9	1·2	1·1	1·4	1·5	1·0	2·0	2·3	1·4	1·3	0·8	0·7	1·1
Yb	3·6	0·7	0·8	1·1	1·2	1·1	1·6	1·1	1·6	2·2	1·1	1·3	0·9	0·9	0·8
Lu	0·6	0·1	0·1	0·1	0·2	0·2	0·2	0·2	0·2	0·3	0·2	0·2	0·2	0·2	0·2
$(La/Sm)_N$	0·08	0·13	0·20	0·27	0·23	0·11	0·11	0·18	0·18	0·28	0·14	0·13	0·40	0·13	0·07
$(La/Yb)_N$	0·07	0·09	0·12	0·20	0·13	0·15	0·09	0·13	0·13	0·21	0·10	0·10	0·38	0·11	0·07
Y/Sr	3·7	1·4	1·2	2·0	1·7	1·7	2·3	1·8	2·0	3·9	2·2	2·1	1·7	1·6	2·0
Magma type	DB	DB	DB	KB	KB	KO	KO	KO	KO	EB	DB	DB	EB	DB	DB

Sample no.:	BW414	BW416	BW495	BX001	BX076	BX122	BX126	BX153	BX155	BX211	BX215	BX227	BX240	BX244	BX248
Lithology:	basalt	basalt	Kbasalt	komatiite	basalt	basalt	basalt	Dbasalt	basalt	Ebasalt	basalt	basalt	Dbasalt	basalt	Dbasalt
Texture:	euhedral	euhedral	spinifex	spinifex	spinifex	spinifex	euhedral	euhedral	euhedral	euhedral	spinifex	spinifex	spinifex	spinifex	spinifex
Locality:	ES2	ES2	WM	EM	ES2	WN	WN	WN	WN	EN	EN	EN	EN	EN	EN
Distance:	740	680	−110	−530	1840	520	1180	2560	2780	2740	2610	1910	1450	1210	1120
SiO_2	54·6	53·3	53·8	51·1	53·4	52·6	53·9	53·6	53·3	53·6	53·0	50·0	52·1	51·7	52·5
TiO_2	0·3	0·5	0·2	0·4	0·2	0·4	0·3	0·3	0·4	0·3	0·4	0·5	0·6	0·4	0·5
Al_2O_3	1·4	2·4	3·0	5·1	2·6	3·2	2·1	2·1	2·2	2·7	2·9	8·2	3·9	4·2	3·5
Cr_2O_3	0·9	0·0	0·3	0·4	0·1	0·1	0·0	0·2	0·0	0·0	0·1	0·1	0·2	0·2	0·3
FeO	5·7	9·5	6·4	8·3	10·5	11·2	8·5	10·9	10·8	9·4	10·9	6·8	9·5	10·1	10·1
MnO	0·1	0·2	0·1	0·2	0·2	0·2	0·1	0·1	0·2	0·3	0·2	0·2	0·2	0·3	0·3
MgO	17·7	16·0	18·9	14·3	15·9	15·6	16·4	17·6	15·5	18·0	16·8	16·1	14·7	15·9	16·1
CaO	18·7	17·6	16·8	19·9	17·0	16·3	18·3	14·6	17·3	15·6	15·3	17·6	18·3	17·0	16·3
Na_2O	0·5	0·5	0·3	0·2	0·2	0·1	0·3	0·4	0·3	0·1	0·2	0·4	0·2	0·2	0·3
Sr	38	26	5·7	8·3	3·9	7·3	5·3	4·8	10	3·7	4·2	6·1	10	8·9	7·8
Y	10	23	10	18	20	20	18	15	24	16	25	28	27	33	20
Zr	12	25	7·5	15	8·3	13	5·9	6·2	10	11	26	39	28	34	17
Nb	0·022	0·002	0·006	0·010	0·001	0·003	0·001	0·005	0·004	0·002	0·003	0·009	0·011	0·010	0·008
Ba	0·1	0·0	0·0	0·2	0·1	0·4	0·2	0·1		0·1	0·8	0·4	0·0	0·4	0·3
La	1·1	2·2	0·2	0·4	0·4	0·2	0·3	0·1	0·2	0·5	0·4	0·7	0·4	0·7	0·3
Ce	3·7	7·9	0·9	1·4	1·4	1·2	0·9	0·7	1·4	1·4	1·8	2·5	1·7	2·5	1·2
Pr	0·8	1·5	0·2	0·3	0·3	0·4	0·2	0·2	0·4	0·3	0·3	0·5	0·4	0·5	0·3
Nd	5·4	9·2	1·3	2·5	1·9	2·3	1·3	1·5	2·8	1·9	2·3	3·9	3·5	3·4	2·8
Sm	1·8	3·2	0·7	1·3	1·0	1·7	1·2	0·7	1·2	1·2	1·2	1·6	1·8	1·6	1·0
Eu	0·6	1·1	0·3	0·5	0·3	0·5	0·3	0·3	0·5	0·3	0·3	0·6	0·7	0·6	0·4
Gd	1·9	3·9	0·8	2·0	1·9	1·9	1·8	1·5	2·4	1·6	1·8	3·7	3·1	2·9	2·1
Dy	1·8	4·0	1·5	2·8	2·8	3·5	2·9	2·1	3·4	2·4	3·0	4·1	4·3	4·9	3·0
Er	0·9	1·5	0·9	2·3	1·8	2·1	1·8	1·4	2·0	1·6	2·8	2·6	2·6	3·9	2·0
Yb	1·0	2·0	1·0	1·8	2·1	2·3	1·4	1·5	1·8	1·6	4·2	3·0	2·5	3·9	1·9
Lu	0·2	0·3	0·2	0·3	0·3	0·4	0·2	0·2	0·3	0·2	0·8	0·5	0·4	0·5	0·3
$(La/Sm)_N$	0·38	0·45	0·18	0·22	0·24	0·09	0·14	0·14	0·13	0·26	0·22	0·29	0·15	0·29	0·20
$(La/Yb)_N$	0·73	0·80	0·15	0·17	0·13	0·07	0·14	0·07	0·10	0·21	0·07	0·16	0·12	0·13	0·12
Y/Sr	0·3	0·9	1·7	2·1	5·0	2·8	3·4	3·1	2·4	4·2	5·9	4·6	2·7	3·7	2·5
Magma type	EB	EB	KB	KO	EB	DB	DB	DB	DB	EB	EB	EB	DB	EB	DB

Locality and distance (in m) are explained in Fig. 1 and Table 1, respectively. KO, DB, KB and EB indicate komatiite, D-basalt, komatiitic basalt and E-basalt, respectively. Subscript N denotes chondrite-normalized values. SiO_2 to Na_2O in wt %; Sr to Lu in ppm.

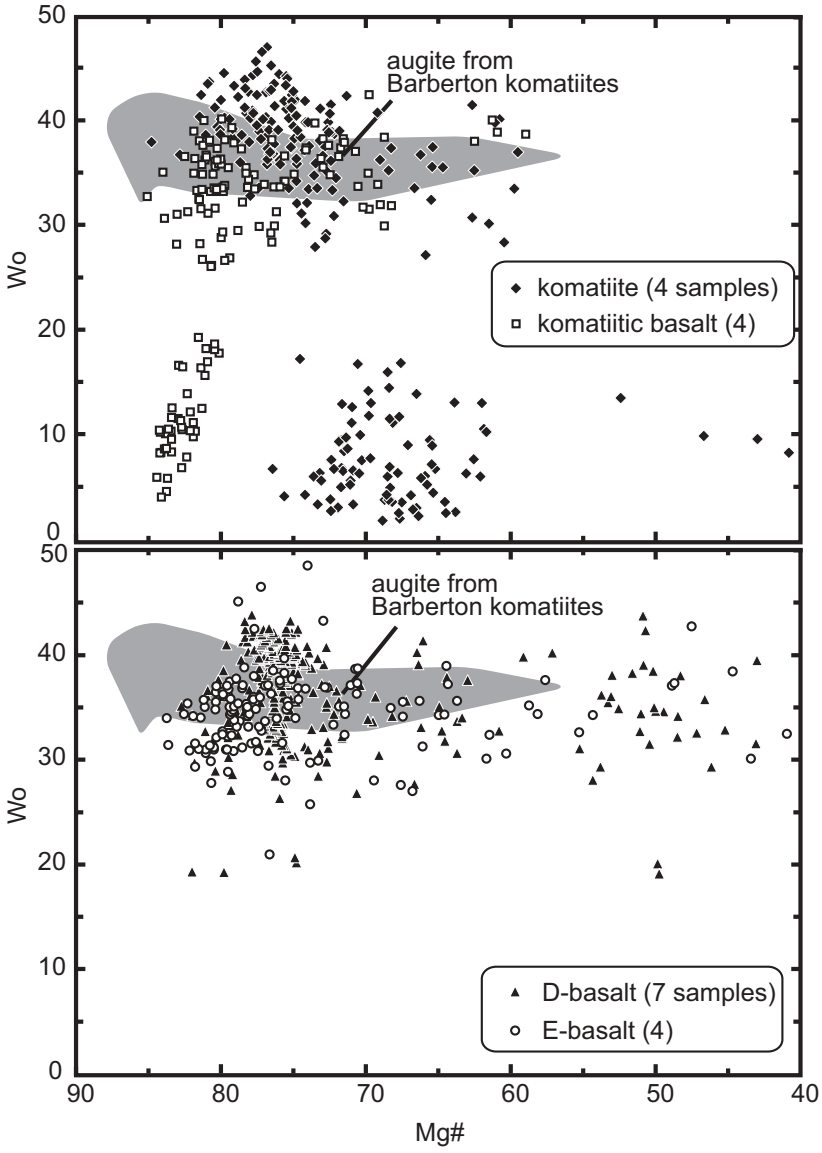

Fig. 8. Wollastonite content (mol %) vs Mg-number [= 100Mg/(Mg + Fe^{total})] of clinopyroxene in the Belingwe volcanic rocks. The compositions of pyroxenes in the komatiites and komatiitic basalts are shown in the upper diagram; those in the D-basalts and E-basalts are shown in the lower diagram. The gray shaded field represents the compositions of augite in Barberton komatiites compiled from Parman *et al.* (1997).

estimated by olivine addition to the least-altered spinifex-textured komatiites to 25·7 wt % MgO (Table 4; Fig. 11), which is in equilibrium with the most magnesian olivine reported in the Belingwe komatiite (Fo = 93·5; Shimizu *et al.*, 2001). The calculation assumed an olivine–melt Fe–Mg partition coefficient of 0·32 and that the Fe^{3+} content of the melt was 10% of the total Fe. Second, an AFC trend was calculated from the estimated parental komatiite. In this model, the compositions of the crustal contaminants and the degree of crustal assimilation were regarded as unknown values, which were derived by minimizing the major element compositional differences between average contaminated basalts and calculated AFC melts. The trace element and isotope compositions of the contaminants were then evaluated using a similar AFC approach based on the degrees of AFC that resulted from the calculation of major element compositions.

Komatiite and D-basalt

The compositional trends for komatiite can be derived by simple crystallization or accumulation of olivine from the primary komatiite, whereas that of the D-basalts may require clinopyroxene fractionation because the CaO/Al_2O_3 ratios of D-basalts are substantially lower than those of komatiites (Fig. 11). Different crystallization

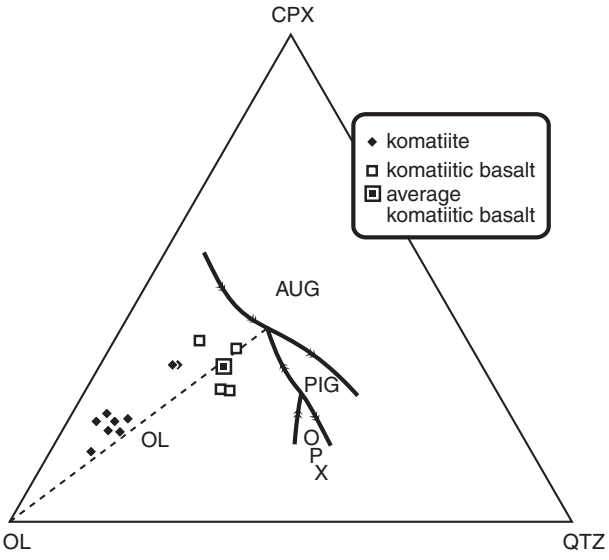

Fig. 9. The bulk compositions of komatiites and komatiitic basalts from the Belingwe greenstone belt plotted in the olivine (OL)–clinopyroxene (CPX)–quartz (QTZ) pseudo-ternary. One-atmosphere liquidus relationships are shown from Kinzler & Grove (1985). The dashed line from OL to the reaction point is the compositional boundary in the olivine liquidus field that determines whether augite (above) or pigeonite (below) crystallizes as the first pyroxene. Arrows on the cotectic curves represent the direction of falling temperature.

sequences between low- and high-SiO_2 basalts may be attributed to variable crystallization depths. The effect of increasing pressure under anhydrous conditions in the basaltic system (e.g. Takahashi & Kushiro, 1983) is to shrink the olivine liquidus field and expand the orthopyroxene and clinopyroxene stability fields. Thus, high-SiO_2 D-basalts could have crystallized at relatively shallower depths than low-SiO_2 basalts. D-basalts (or komatiite-related tholeiitic basalts) are the most voluminous lava in Archean greenstone belts (e.g. Arndt *et al.*, 1997). Although these basalts can be formed either from melting of depleted mantle at low-pressure conditions or by fractional crystallization of ultramafic komatiite, it is usually difficult to distinguish between these two possibilities using geochemical data. In the case of this study, we interpret the Belingwe greenstone belt as having formed in an autochthonous intra-continental setting. Therefore, mantle melting at low pressure is unlikely to occur, because a thick continental crust would block the mantle from ascending to a shallow depth. Thus, we favor the latter case, that a significant proportion of the komatiitic magma fractionally crystallized before reaching the surface, and that the D-basalts erupted as relatively evolved magmas (Anhaeusser, 1985). The slight enrichment of Nd isotopic ratios in the D-basalts and the lower Nb/U ratios of some komatiites and D-basalts may be attributed to a very small degree (<1% contamination) of crustal contamination (Fig. 12).

Komatiitic basalt and E-basalt

Komatiitic basalts are enriched in both LREE and radiogenic isotopic compositions, and their chemical characteristics, including high SiO_2 and MgO contents, are similar to those of siliceous high magnesian basalts (SHMB), which have been suggested to be derived by crustal contamination of komatiite magmas (e.g. Redman & Keays, 1985; Arndt & Jenner, 1986; Barley, 1986; Sensarma *et al.*, 2002). Alternatively, Cameron *et al.* (1979) and Grove & Parman (2004) have suggested that the composition and texture of these volcanics resemble those of boninites, implying that they were derived by melting of hydrated refractory mantle peridotite in a subduction environment. Arndt (2003) indicated the difficulty in distinguishing between magmas that have assimilated crustal rocks from magmas formed in subduction settings.

Although the E-basalts in the Belingwe greenstone belt are also enriched in LREE and have isotopic compositions similar to the komatiitic basalts, they display slightly U-shaped REE patterns that are similar those of boninites (Fig. 4). Boily & Dion (2002) reported volcanic rocks with U-shaped REE profiles from the ~2·8 Ga Superior Province, Canada. Taking into account that these rocks conformably overlie lava flows of calc-alkaline basaltic to dacitic rocks, they concluded that the volcanic sequence originated in a subduction environment. Because felsic units are entirely absent from the Belingwe greenstone belt (e.g. Nisbet *et al.*, 1993*b*), and because the compositions of the Belingwe komatiites and D-basalts do not show any subduction features, the E-basalts are unlikely to have originated at a convergent margin. Similar boninite-like rocks in an intra-continental setting occur in the ~3·0 Ga Mallina Basin, Pilbara Craton (Smithies, 2002; Smithies *et al.*, 2004). Their setting is similar to that of the Ngezi volcanic sequence in this study. Smithies *et al.* (2004) suggested that the boninite-like rocks were unlikely to be formed by crustal assimilation, because the magmatic rocks show a remarkably narrow range in incompatible trace elements (Fig. 4), despite having been intruded through compositionally diverse continental crust. Smithies *et al.* (2004) concluded that the Pilbara boninite-like rocks were formed by melting of a homogeneous refractory hydrated mantle source that had been metasomatically enriched by an earlier subduction event. Although the enriched signatures of the E-basalts in the Belingwe greenstone belt could have been derived from a refractory enriched source mantle, we favor the crustal assimilation model for their petrogenesis because the compositional diversity of the E-basalts (Fig. 4) may be related to the compositional variations in the crustal assimilants. The recent discovery of lower crustal garnets in the komatiites (Shimizu *et al.*, 2004) also provides strong evidence for crustal assimilation.

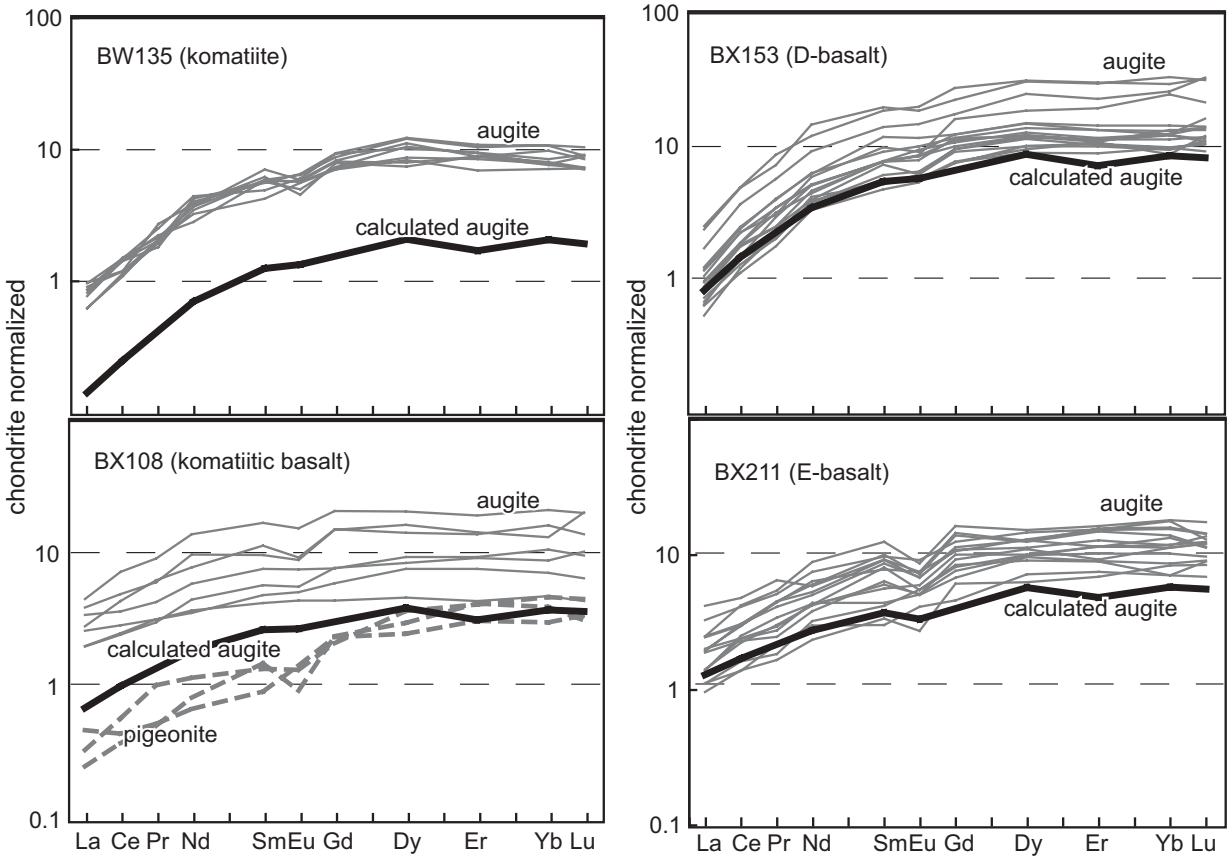

Fig. 10. Chondrite-normalized rare earth element patterns of clinopyroxene in samples of komatiite, komatiitic basalt, D-basalt and E-basalt. SIMS REE patterns for augite and pigeonite are shown by gray continuous and dashed lines, respectively. Bold black lines indicate the compositions of augite calculated to be in equilibrium with the respective whole-rock compositions using the clinopyroxene–melt partition coefficients of Hart & Dunn (1993).

The different μ1 values for the Belingwe komatiitic basalts and E-basalts cannot be derived from a single contaminant using a simple AFC calculation, if it is assumed that their parental magmas had similar Pb and U concentrations. Therefore, two sources of contamination were assumed, as shown in Figs 11 and 12 and Table 4. Although the calculated degrees of assimilation for the komatiitic basalts and E-basalts are high at 20% and 30%, respectively, these values are consistent with those derived from the numerical simulations of Huppert & Sparks (1985). When high-temperature komatiitic magmas are intruded turbulently through continental crust, considerable heat is transferred to the crust, causing extensive melting. The major element compositions of the calculated contaminant for the komatiitic basalt are similar to those of Archean granite (Fig. 10). The relatively high ratios of $(La/Sm)_N$ and $(La/Yb)_N$ in the komatiitic basalt contaminant (Fig. 11) may also indicate that it contained a major component of Archean granite, similar in composition to the Archean upper crust of Taylor & McLennan (1995). Compared with this, the E-basalt contaminant is relatively mafic (MgO $\sim$ 5·0 wt %; Fig. 11) and has a lower $(La/Yb)_N$ ratio (Fig. 11), indicating that the E-basalts were derived by contamination with a more mafic crust. However, the estimated compositions of the contaminants do not appear to be ordinary continental crust, as shown, in particular, by the slightly U-shaped REE profile of the calculated contaminant [$(La/Sm)_N$ 2·4; $(Gd/Yb)_N$ 0·8] for the E-basalt. The contaminants required to form the komatiitic basalt and the E-basalt may not only represent upper continental crust but may potentially include variable proportions of middle and lower continental crust, a subcontinental lithospheric mantle component, such as a lamprophyre, or even sedimentary rocks at the base of the volcanic sequence (the Manjeri Formation). As the contaminants appear to be the consequence of mixing of these crustal materials in certain ratios, the U-shaped pattern of the contaminant for the E-basalt can be derived by a simple mixture of $\sim$70% LREE-depleted lower continental crust [such as represented by pyroxene-rich xenoliths of Rudnick *et al.* (1986)] and $\sim$30% of an ordinary Archean granitic rock (see Martin, 1986) or the basement granite

Table 4: Compositions used for the various components in the assimilation–fractional crystallization calculations, and calculated composition of potential contaminants

Sample	Estimated primary komatiite	Average of komatiitic basalt	Average of E-basalt	Contaminant for komatiitic basalt ($R = 0{\cdot}6$, $A = 20{\cdot}7\%$)	Contaminant for E-basalt ($R = 0{\cdot}8$, $A = 31{\cdot}2\%$)	Archean upper crust*	Archean bulk crust*
wt %							
SiO_2	48·0	55·1	55·0	68·8	60·6	60·0	57·0
TiO_2	0·34	0·57	0·55	0·76	0·56	0·83	1·0
Al_2O_3	7·0	11·8	14·1	17·0	20·3	15·3	15·2
FeO	11·0	9·8	8·8	2·7	3·1	8·0	9·6
MgO	25·7	11·4	9·5	1·1	5·0	4·7	5·9
CaO	7·0	8·0	9·3	0·80	5·8	6·2	7·3
$Na_2O + K_2O$	1·0	3·2	2·6	8·9	4·6	5·1	3·9
ppm							
Sr	29·7	91·0	84·2	257	161	240	215
Zr	13·6	39·5	38·0	108	72·0	125	100
Nb	0·52	1·5	1·3	3·9	2·2	4·0	2·1
La	0·68	3·1	3·3	11	8·1	20	15
Nd	1·7	4·6	4·4	12	7·6	20	16
Sm	0·62	1·4	1·4	3·0	2·1	4·0	3·4
Gd	0·88	1·7	1·9	3·1	2·9	3·4	3·2
Dy	1·2	2·1	2·6	3·5	4·0	3·4	3·6
Yb	0·78	1·4	1·8	2·1	2·9	2·00	2·20
Pb	0·15	0·98	1·5	3·7	4·0	—	—
Th	0·059	0·97	1·1	4·1	3·2	5·7	2·9
U	0·022	0·32	0·34	1·3	0·97	1·5	0·75
εNd	2·1	0·70	−0·35	−0·37	−2·2	—	—
μ1	8·1	8·4	9·0	8·5	9·1	—	—
T_{DM}				2·8 Ga	3·3 Ga		

*Taylor & McLennan (1995).
R, ratio of assimilation and fractional crystallization; *A*, degree of assimilation.

surrounding the Belingwe greenstone belt (Luais & Hawkesworth, 1994).

T_{DM} model ages (DePaolo, 1981) of the contaminants for the komatiitic basalt and the E-basalt were calculated to be ~2·8 Ga and ~3·3 Ga, respectively, using the estimated Sm and Nd concentrations and εNd from Table 4; the model ages of the contaminants are slightly younger than, but are consistent with, those of the surrounding crustal basement. The μ1 values of the contaminants are also consistent with those of the coeval gneisses and granitoids from the Zimbabwe Craton (2·9 Ga: μ1 = 8·1–8·5; 3·5 Ga: μ1 = 8·8–9·0; Taylor *et al.*, 1991).

RECONSTRUCTION OF THE VOLCANIC STRATIGRAPHY

As discussed above, the Belingwe volcanics can be subdivided into four rock types based on their petrology and geochemistry. Chemical variations within the komatiites and D-basalts are easily explained by crystal fractionation from primary komatiite, whereas those of the komatiitic basalts and E-basalts can be derived by assimilation of crustal material by the komatiitic magmas. To discuss the eruptive history of the Belingwe volcanic sequence, a detailed stratigraphy of the volcanic sequence is required. To reconstruct the volcanic stratigraphy, a significant number of fresh samples from a wide area must be assessed for all magma types. However, most volcanic rocks from the Belingwe greenstone belt are altered and metamorphosed, thus their whole-rock compositions may not represent the original igneous composition (e.g. Lahaye & Arndt, 1996). Recently, Parman *et al.* (2003) suggested that clinopyroxene preserves pre-metamorphic trace element compositions even in metamorphosed komatiitic rocks. We have also shown that the REE patterns of augite in each magma type are distinct from one

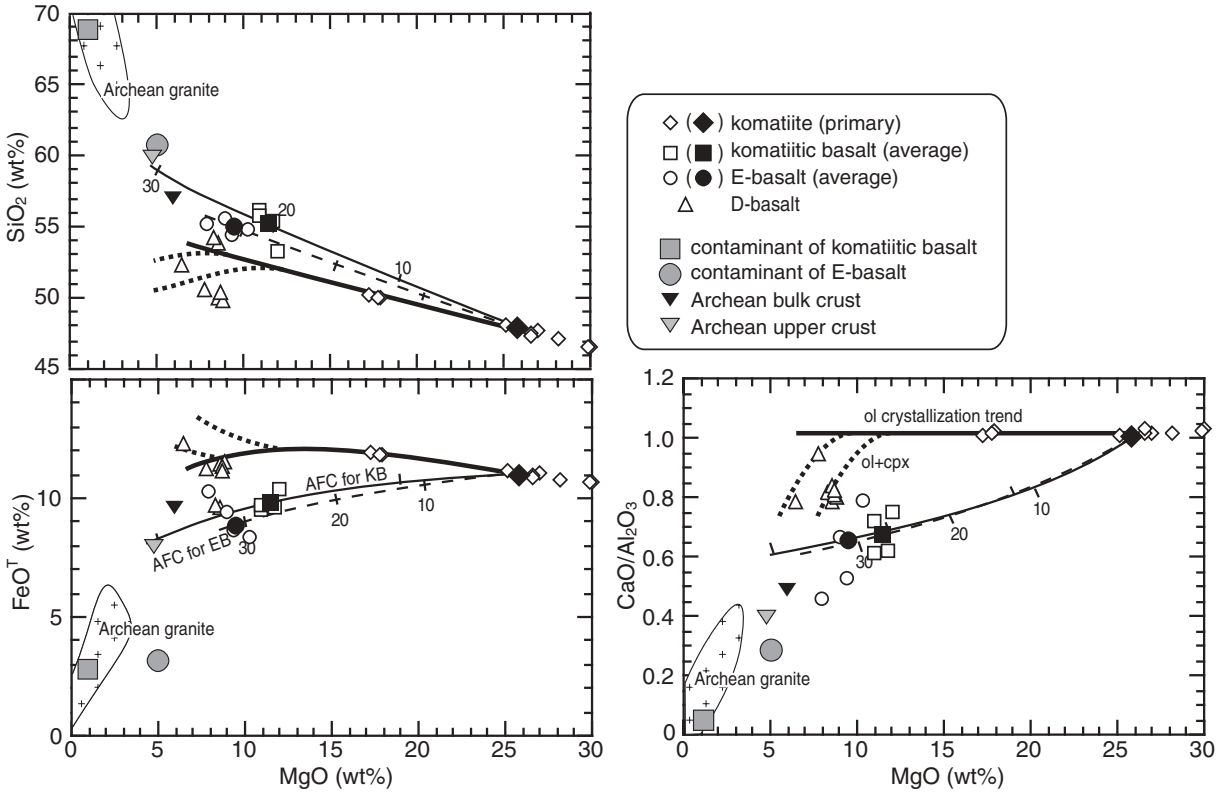

Fig. 11. MgO (wt %) variation diagrams showing the compositions of the Belingwe volcanics, potential contaminants, Archean granites (Martin, 1987; Martin *et al.*, 1983), and the average Archean bulk and upper crust of Taylor & McLennan (1995). Model curves are shown for: fractional crystallization of olivine alone (bold continuous line) and of olivine + clinopyroxene (bold dotted line); AFC for komatiitic basalt (fine continuous line) and for E-basalt (dashed line; see Appendix). Tick marks on the mixing lines indicate the degree of assimilation in per cent.

another (Fig. 9). Therefore, we have used the trace element compositions of clinopyroxene relicts to divide these highly altered samples into the four magma types mentioned above.

Clinopyroxene geochemistry

As shown in Figs 9 and 13, the trace element compositions of clinopyroxene are variable within each type of volcanic rock. The positive correlations between La content and La/Sm ratio in augite from the komatiites and D-basalts may be attributed to augite fractionation, because the compositional variations of the augite in these samples are similar to those predicted from Rayleigh fractionation trends (Fig. 13). However, augites from the komatiitic basalt and E-basalt do not exibit correlations between La abundance and La/Sm ratio. This may reflect the trace element heterogeneity of the magmas from which these pyroxenes crystallized, as a result of either rapid crystal growth or crustal contamination. Even though the La/Sm ratios of the augites in the contaminated rocks (komatiitic basalt and E-basalt) are scattered, they tend to be higher than those in the less contaminated rocks (komatiite and D-basalt; Figs 13 and 14a). We are able to use certain trace element ratios (i.e. La/Sm, La/Yb, Y/Sr) in pyroxene to distinguish two magma types (enriched and depleted; Fig. 14a). However, more than three pyroxene analyses are required for an unknown sample to clearly suggest its magma type as shown in Fig. 14b, because the compositional fields of the contaminated and uncontaminated rocks overlap.

Volcanic stratigraphy

Taking into account the composition of the whole rocks and clinopyroxene, the stratigraphy of the 2·7 Ga Belingwe volcanic sequence can be elucidated as shown in Fig. 15. Because of the limited exposure of the volcanic sequence, and the variable degrees of clinopyroxene preservation, we could not obtain the complete volcanic stratigraphy from a single traverse. Allowing for these constraints, the reconstructed volcanic stratigraphy is given as Fig. 15.

At the base of the volcanic sequence in the Reliance Formation, less contaminated basalts (D-basalts) dominate. However, the magma type of the volcanic rocks at the Manjeri–Reliance Formation boundary has

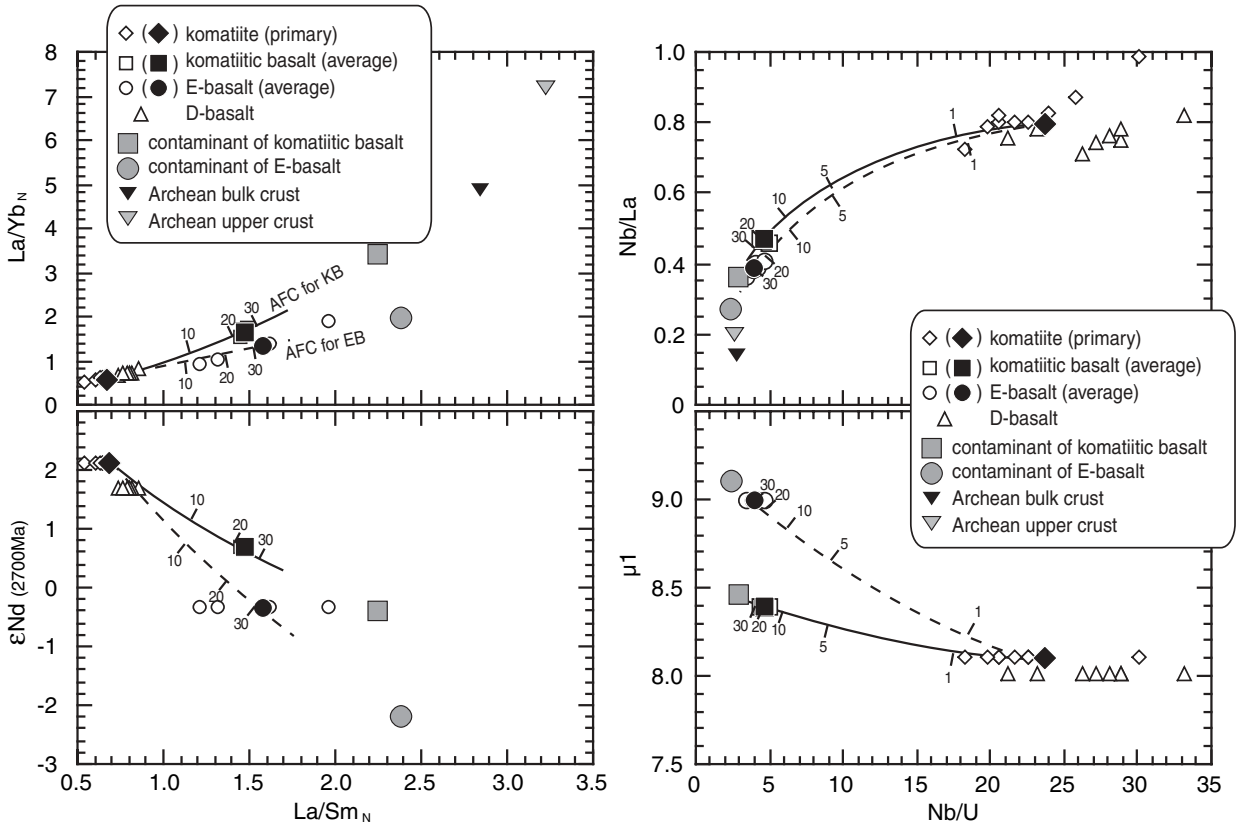

Fig. 12. Trace element ratios and isotope composition variation diagrams for the Belingwe volcanics, potential contaminants, Archean granites, and the average Archean bulk and upper crust of Taylor & McLennan (1995). Model curves are AFC for komatiitic basalt ($R = 0{\cdot}6$; continuous line) and AFC for E-basalt ($R = 0{\cdot}8$; dashed line; see Appendix). Tick marks on the mixing lines indicate degrees of assimilation in per cent. N denotes chondrite-normalized value (McDonough & Sun, 1995).

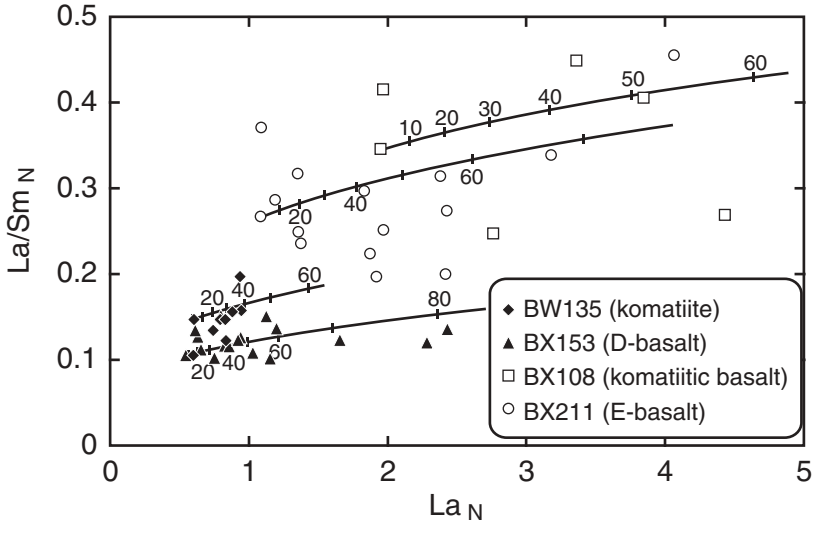

Fig. 13. Variation of $(La/Sm)_N$ vs La_N for augite from the Belingwe volcanic rocks. N denotes chondrite-normalized value (McDonough & Sun, 1995). Lines with tick marks show a Rayleigh fractionation path calculated using the clinopyroxene–melt partition coefficients of Hart & Dunn (1993), starting from a melt that is in equilibrium with the lowest La content augite in each sample. Each tick mark represents 10% clinopyroxene crystallization.

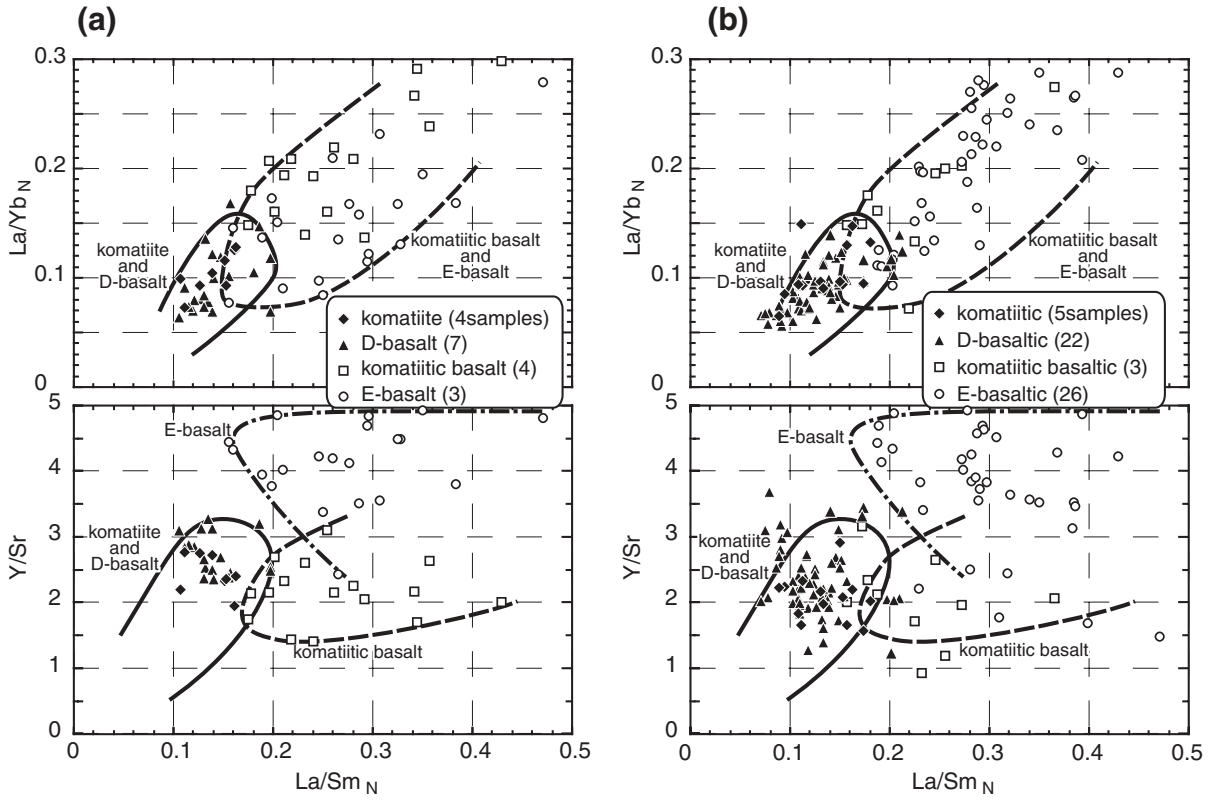

Fig. 14. Variation diagrams for trace element ratios in augite relicts within: (a) samples classified from the whole-rock compositions, showing that the compositional boundaries between komatiite and D-basalt and komatiitic basalt and E-basalt can be determined, and (b) samples classified by the clinopyroxene compositions using compositional boundaries determined in (a). Augite analyses with Ba > 0·5 ppm were disregarded because of the possibilities of analyzing cracked or altered parts of grains.

not been determined because of the absence of clinopyroxene relicts within these rocks. Above this D-basalt flow, highly contaminated komatiitic basalts occur. This stratigraphy is observed at two localities (ES1 and ES2; Fig. 15). The least contaminated and least fractionated komatiite flow lies between contaminated komatiitic basalts. Above the uppermost komatiitic basalt flow in the Reliance Formation, komatiites or komatiitic basalts are absent. The Zeederbergs Formation is composed of dominantly basaltic rocks. Such a stratigraphy for komatiite–basalt occurrences is common for Archean greenstone belts (e.g. Sylvester *et al.*, 1997). The number of analyzed D-basalts and E-basalts in the Zeederbergs Formation is 23 and 26, respectively. Hofmann *et al.* (2003) also reported this alternation of D- and E-basaltic flows using REE profiles of basaltic rocks along the main river that cuts the Zeederbergs Formation. They proposed that the Zeederbergs Formation has been tectonically duplicated, based on the observations of a stratigraphic repetition related to thrusting of the uppermost sedimentary sequence (Hofmann *et al.*, 2001*a*). However, alternating flows could be also produced by simple alternate eruptions of D- and E-basalts, which can be derived by replenishment of komatiite melt into a magma chamber. Repetitions of geochemical variations are common in Phanerozoic continental flood basalt sequences (e.g. Hooper & Hawkesworth, 1993; Marsh *et al.*, 1997). As a result of the poor exposure of the Zeederbergs Formation, clear geological evidence for reconstructing the tectonic environment of the Zeederbergs Formation is not preserved. Because the Ngezi volcanic rocks were erupted directly onto continental crust (e.g. Bickle *et al.*, 1994; Shimizu *et al.*, 2004), it is not likely that a major tectonic thrusting event deformed the Zeederbergs volcanic units soon after eruption. Therefore, the alternation of D- and E-basaltic flows within the Zeederbergs Formation is probably due to the simple alternate eruptions of these basalts.

SUMMARY AND IMPLICATIONS FOR THE EVOLUTION OF THE BELINGWE GREENSTONE BELT

The geochemistry and stratigraphic reconstructions of the 2·7 Ga volcanic sequence can be used to constrain the evolution of the Belingwe greenstone belt.

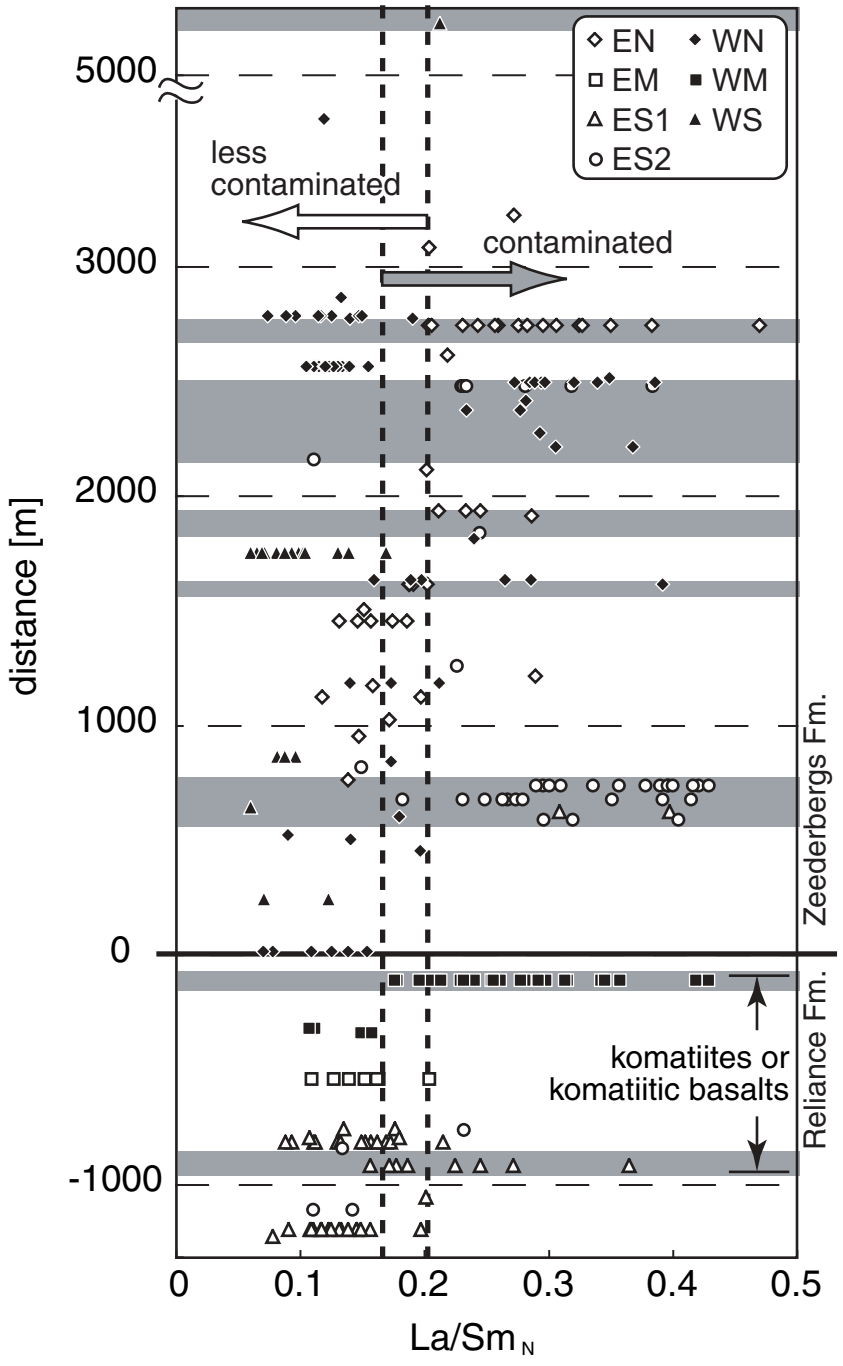

Fig. 15. The stratigraphy of contaminated and uncontaminated volcanics, as determined by the $(La/Sm)_N$ ratios of clinopyroxene at each locality compared with the stratigraphy of the 2·7 Ga Belingwe volcanic sequence. Each symbol indicates the sampling localities shown in Fig. 1. The 'distance' parameter plotted as the vertical axis is explained in Table 1. The bold continuous line at 0 m indicates the boundary between the Reliance and Zeederbergs Formations. The gray and white layers indicate schematically the contaminated and less contaminated horizons, respectively.

Four types of volcanic rocks, based on petrography and geochemistry, occur in the 2·7 Ga Ngezi volcanic sequence. Komatiites and D-basalts are slightly depleted in both their isotopic and trace element compositions. Chemical variations in the komatiites and D-basalts were primarily due to mainly fractional crystallization of olivine and minor pyroxene from a primary komatiitic magma. Very small amounts of crustal assimilation are detected by certain trace element ratios (e.g. lower Nb/U) and Pb isotopic compositions. Komatiitic basalts and

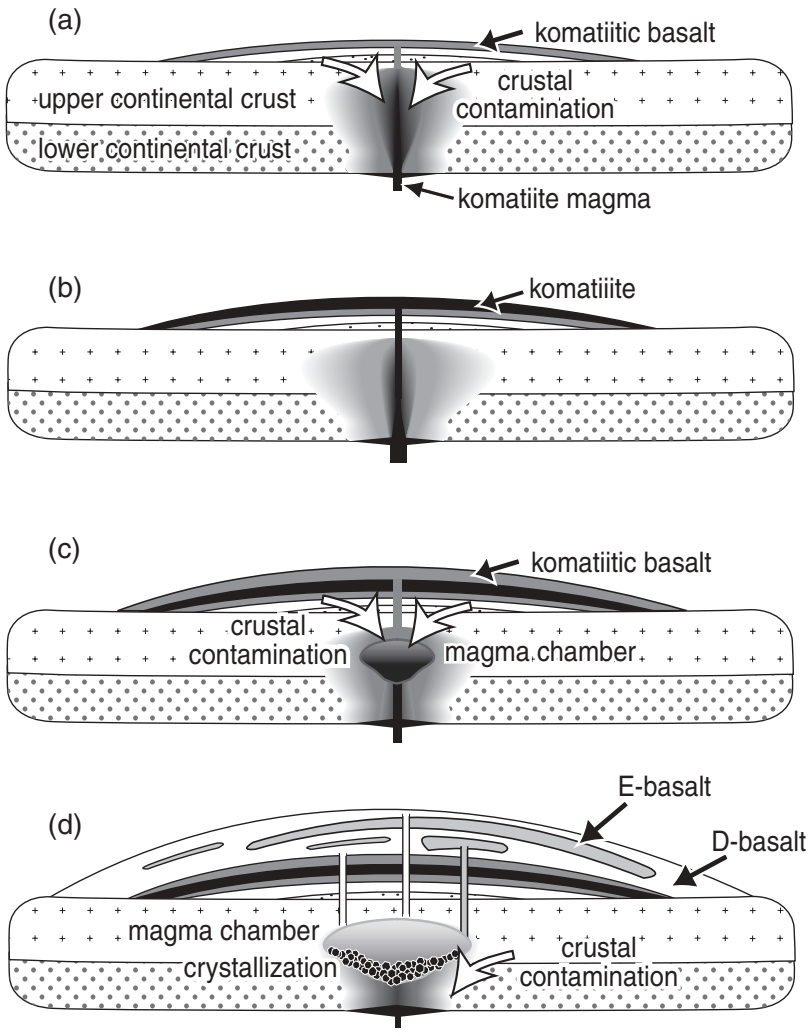

Fig. 16. Schematic diagrams illustrating the evolution of the 2·7 Ga volcanic sequence in the Belingwe greenstone belt. (a) Early komatiitic basalt eruption. (b) Komatiite eruption. (c) Later komatiitic basalt eruption. (d) E-basalt and D-basalt eruptions.

E-basalts are more siliceous and have more radiogenic isotopic and trace element compositions. Their chemical trends can be derived by AFC from a primary komatiite. AFC calculations indicate that the chemical differences between the E-basalts and komatiitic basalts could be due to variable degrees of crustal assimilation and contaminants of different composition. The E-basalts were derived by a higher degree of contamination from a more mafic crustal component than the komatiitic basalts.

The volcanic stratigraphy of the Ngezi sequence indicates that komatiites and komatiitic basalts are restricted to near the base of the succession, and that basalts predominate throughout the sequence. The least contaminated komatiite lies between highly contaminated komatiitic basalts. Contaminated basalts appear to have erupted in similar volumes to the less contaminated basalts.

Based on our results, and an improved understanding of the physical volcanology of magma emplaced into continental crust (e.g. Huppert & Sparks, 1985; Campbell & Turner, 1987; Campbell & Hill, 1988), we interpret the evolution of the 2·7 Ga Belingwe volcanic sequence as shown in Fig. 16. A considerable amount of komatiitic magma was produced during a high-degree melting event in a mantle plume of extraordinary high temperature (~1800°C) at a depth of ~150 km (~5 GPa under anhydrous conditions; e.g. Herzberg & Zhang, 1996). Even if the Belingwe komatiites originated under hydrous conditions ($H_2O \sim 0{\cdot}9$ wt % in primary magma; Shimizu *et al.*, 2001), komatiites still require a high temperature to be formed. For example, the presence of 1 wt % H_2O in the mantle decreases the temperature for komatiite generation by only ~100°C (Asahara & Ohtani, 2001), thus a hot mantle plume is still required. Assuming that the komatiitic magma migrated through continental crust with a typical structure, the komatiite magma may stagnate at the upper–lower crust boundary

because here the density of the Belingwe komatiitic magma (2·72 g/cm^3 at an anhydrous condition; Agee & Walker, 1993) is lower than that of the lower continental crust (~3·0 g/cm^3), but higher than that of upper continental crust (~2·65 g/cm^3). For komatiite eruptions in an intracontinental setting, Huppert & Sparks (1985) have suggested that exceptionally high flow rates are required. During the early stages of magmatism, the high-temperature komatiite magmas could have assimilated upper continental crust extensively to form the contaminated komatiitic basalts (Fig. 16a). The temperature of the lower crust, however, may not have been high enough at this stage for it to be easily assimilated by the komatiites. As the magma flow rate increased and the volcanic conduits became wider, the komatiite magma erupted through the crust without major assimilation or crystal fractionation (Fig. 16b). The magmatic activity should be its peak at this stage. As the magmatic activity decreased with time, the komatiitic magmas would have stagnated in the continental crust and magma chambers were formed (Fig. 16c). The komatiite thermally assimilates upper continental crust in the upper part of the magma chamber, forming komatiitic basalt. During the later stages, the komatiite is contaminated mainly with lower continental crust, thus forming E-basalts as the temperature of the lower crust becomes high enough for it to be partially melted by the continuous supply of heat from the rising komatiitic magma. At the same stage, the komatiites fractionally differentiated within the magma chamber to form the D-basalts (Fig. 16d). In this model, considerably thick cumulate layers would form at the bottom of the magma chambers because of the substantial volumes of basalt in the Nzegi volcanic sequence. Prendergast (2004) showed that dunite and pyroxenite layers occur in a broad area within the Belingwe greenstone belt, which we regard to be the cumulate layers formed at shallow depths within the crustal magma chambers. The chemical compositions of most of the volcanic rocks in the Nzegi volcanic sequence are derived by a combination of crystallization–differentiation and crustal assimilation of a parental komatiite melt.

ACKNOWLEDGEMENTS

We are grateful to K. Hirose and T. Komiya for the field survey and constructive discussions throughout this study. We are indebted to T. Kuritani, K. Kobayashi, C. Sakaguchi, R. Tanaka, A. Makishima and all the other Pheasant Memorial Laboratory members for their analytical support and helpful suggestions. The manuscript was considerably improved by the reviews from R. Sproule and A. Kerr, and by comments from I. Campbell. R. King and I. Buick are also acknowledged for improving the manuscript. The editorial encouragement and review from N. Arndt is gratefully acknowledged. This study was financially supported by fellowships from the Japan Society for the Promotion of Science for Japanese Junior Scientists (to K.S.), by grants from the Ministry of Education, Culture, Sports, Science and Technology of Japan (to E.N.) and by the program of 'Center of Excellence for the 21st Century in Japan' (to E.N.).

REFERENCES

Agee, C. B. & Walker, D. (1993). Olivine flotation in mantle melt. *Earth and Planetary Science Letters* **114**, 315–324.

Anhaeusser, C. R. (1985). Archean layered ultramafic complexes in the Barberton Mountain Land, South Africa. In: Ayres, L. D., Thurston, P. C., Card, K. D. & Weber, W. S. (eds) *Evolution of Archean Supracrustal Sequences*. Toronto, Ont: Geological Association of Canada, pp. 281–301.

Arndt, N. T. (1994). Archean komatiites. In: Condie, K. C. (ed.) *Archean Crustal Evolution*. Amsterdam: Elsevier, pp. 11–44.

Arndt, N. T. (2003). Komatiites, kimberlites and boninites. *Journal of Geophysical Research* **108**(B6), doi:10.1029/2002JB002157.

Arndt, N. T. & Jenner, G. A. (1986). Crustally contaminated komatiites and basalts from Kambalda, Western Australia. *Chemical Geology* **56**, 229–255.

Arndt, N. T., Albarède, F. & Nisbet, E. G. (1997). Mafic and ultramafic magmatism. In: de Wit, M. J. & Ashwal, L. D. (eds) *Greenstone Belts*. Oxford: Oxford University Press, pp. 233–254.

Asahara, Y. & Ohtani, E. (2001). Melting relations of the hydrous primitive mantle in the CMAS–H_2O system at high pressures and temperatures, and implications for generation of komatiites. *Physics of the Earth and Planetary Interiors* **125**, 31–44.

Barley, M. E. (1986). Incompatible element enrichment in Archean basalts: a consequence of contamination by older sialic crust rather than mantle heterogeneity. *Geology* **14**, 947–950.

Bickle, M. J. & Nisbet, E. G. (eds) (1993). *The Geology of the Belingwe Greenstone Belt, Zimbabwe: a Study of Archean Continental Crust. Geological Society of Zimbabwe, Special Publication* **2**.

Bickle, M. J., Martin, A. & Nisbet, E. G. (1975). Basaltic and peridotitic komatiites and stromatolites above a basal unconformity in the Belingwe greenstone belt, Rhodesia. *Earth and Planetary Science Letters* **27**, 155–162.

Bickle, M. J., Arndt, N. T., Nisbet, E. G., Orpen, J. L., Martin, A., Keays, R. R. & Renner, R. (1993). Geochemistry of the igneous rocks of the Belingwe Greenstone Belt: alteration, contamination and petrogenesis. In: Bickle, M. J. & Nisbet, E. G. (eds) *The Geology of the Belingwe Greenstone Belt, Zimbabwe: a Study of Archean Continental Crust. Geological Society of Zimbabwe, Special Publication* **2**, 175–209.

Bickle, M. J., Nisbet, E. G. & Martin, A. (1994). Archean greenstone belts are not oceanic crust. *Journal of Geology* **102**, 121–138.

Blichert-Toft, J., Arndt, N. T. & Gruau, G. (2004). Hf isotopic measurements on Barberton komatiites: effects of incomplete sample dissolution and importance for primary and secondary magmatic signatures. *Chemical Geology* **207**, 261–275.

Boily, M. & Dion, C. (2002). Geochemistry of boninite-type volcanic rocks in the Frotet–Evans greenstone belt, Opatica subprovince, Quebec: implications for the evolution of Archaean greenstone belts. *Precambrian Research* **115**, 349–371.

Bolhar, R., Woodhead, J. D. & Hergt, J. M. (2003). Continental setting inferred for emplacement of the 2·9–2·7 Ga Belingwe Greenstone Belt, Zimbabwe. *Geology* **31**, 295–298.

Cameron, W. E., Nisbet, E. G. & Dietrich, V. J. (1979). Boninites, komatiites and ophiolitic basalts. *Nature* **280**, 550–553.

Campbell, I. H. & Hill, R. I. (1988). A two-stage model for the formation of the granite–greenstone terrains of the Kalgoorlie–Norseman area, Western Australia. *Earth and Planetary Science Letters* **90**, 11–25.

Campbell, I. H. & Turner, J. S. (1987). A laboratory investigation of assimilation at the top of a basaltic magma chamber. *Journal of Geology* **95**, 155–172.

Chauvel, C., Dupre, B. & Arndt, N. T. (1993). Pb and Nd isotopic correlation in Belingwe komatiites and basalts. In: Bickle, M. J. & Nisbet, E. G. (eds) *The Geology of the Belingwe Greenstone Belt, Zimbabwe: a Study of Archean Continental Crust. Geological Society of Zimbabwe, Special Publication* **2**, 167–174.

Condie, K. C. (1998). Episodic continental growth and supercontinents: a mantle avalanche connection? *Earth and Planetary Science Letters* **163**, 97–108.

DePaolo, D. J. (1981). Neodymium isotopes in the Colorado Front Range and crust–mantle evolution in the Proterozoic. *Nature* **291**, 193–196.

Faure, G. (1986). The isotope geology of lead. In: Faure, G. (ed.) *Principles of Isotope Geology*, 2nd edn. New York: John Wiley, pp. 309–340.

Ghiorso, M. S. & Sack, R. O. (1995). Chemical mass-transfer in magmatic processes. 4. A revised and internally consistent thermodynamic model for the interpolation and extrapolation of liquid–solid equilibria in magmatic systems at elevated temperatures and pressures. *Contributions to Mineralogy and Petrology* **119**, 197–212.

Green, T. H. (1994). Experimental studies of trace-element partitioning applicable to igneous petrogenesis—Sedona 16 years later. *Chemical Geology* **117**, 1–36.

Grove, T. L. & Parman, S. W. (2004). Thermal evolution of the Earth as recorded by komatiites. *Earth and Planetary Science Letters* **219**, 173–187.

Hart, S. R. & Dunn, T. (1993). Experimental cpx/melt partitioning of 24 trace elements. *Contributions to Mineralogy and Petrology* **113**, 1–8.

Herzberg, C. & Zhang, J. (1996). Melting experiments on anhydrous peridotite KLB-1: compositions of magmas in the upper mantle and transition zone. *Journal of Geophysical Research* **101**, 8271–8295.

Hofmann, A., Dirks, P. H. G. M. & Jelsma, H. A. (2001*a*). Horizontal tectonic deformation geometries in a late Archaean sedimentary sequence, Belingwe greenstone belt, Zimbabwe. *Tectonics* **20**, 909–932.

Hofmann, A., Dirks, P. H. G. M. & Jelsma, H. A. (2001*b*). Late Archaean foreland basin deposits, Belingwe greenstone belt, Zimbabwe. *Sedimentary Geology* **141–142**, 131–168.

Hofmann, A., Bolhar, R., Dirks, P. H. G. M. & Jelsma, H. A. (2003). The geochemistry of Archaean shales derived from a mafic volcanic sequence, Belingwe greenstone belt, Zimbabwe: provenance, source area unroofing and submarine versus subaerial weathering. *Geochimica et Cosmochimica Acta* **67**, 421–440.

Hooper, P. R. & Hawkesworth, C. J. (1993). Isotopic and geochemical constraints on the origin and evolution of the Columbia River Basalt. *Journal of Petrology* **34**, 1203–1246.

Hunter, M. A., Bickle, M. J., Nisbet, E. G., Martin, A. & Champman, H. J. (1998). Continental extensional setting for the Archean Belingwe Greenstone Belt, Zimbabwe. *Geology* **26**, 883–886.

Huppert, H. E. & Sparks, R. J. (1985). Cooling and contamination of mafic and ultramafic magmas during ascent through continental crust. *Earth and Planetary Science Letters* **74**, 371–386.

Kinzler, R. J. & Grove, T. L. (1985). Crystallization and differentiation of Archean komatiite lavas from northeast Ontario: phase equilibrium and kinetic studies. *American Mineralogist* **70**, 40–51.

Kuritani, T. & Nakamura, E. (2002). Precise isotope analysis of nanogram-level Pb for natural rock samples without use of double spikes. *Chemical Geology* **186**, 31–43.

Kuritani, T. & Nakamura, E. (2003). Highly precise and accurate isotopic analysis of small amounts of Pb using ^{205}Pb–^{204}Pb and ^{207}Pb–^{204}Pb, two double spikes. *Journal of Analytical Atomic Spectrometry* **18**, 1464–1470.

Kusky, T. M. & Kidd, W. S. F. (1992). Remnants of an Archean oceanic plateau, Belingwe greenstone belt, Zimbabwe. *Geology* **20**, 43–46.

Kusky, T. M. & Winsky, P. A. (1995). Structural relationships along a greenstone/shallow water shelf contact, Belingwe greenstone belt, Zimbabwe. *Tectonics* **14**, 448–471.

Lahaye, Y. & Arndt, N. T. (1996). Alteration of a komatiite flow from Alexo, Ontario, Canada. *Journal of Petrology* **37**, 1261–1284.

Lindsley, D. H. (1983). Pyroxene thermometry. *American Mineralogist* **68**, 477–493.

Luais, B. & Hawkesworth, C. J. (1994). The generation of continental crust: an integrated study of crust-forming processes in the Archaean of Zimbabwe. *Journal of Petrology* **35**, 43–93.

Machado, N., Brooks, C. & Hart, S. R. (1986). Determination of initial $^{87}Sr/^{86}Sr$ and $^{143}Nd/^{144}Nd$ in primary minerals from mafic and ultramafic rocks: experimental procedure and implications for the isotopic characteristics of the Archean mantle under the Abitibi greenstone belt, Canada. *Geochimica et Cosmochimica Acta* **50**, 2335–2348.

Makishima, A. & Masuda, A. (1994). Ce isotope ratios of N-type MORB. *Chemical Geology* **118**, 1–8.

Makishima, A. & Nakamura, E. (1997). Suppression of matrix effects in ICP-MS by high power operation of ICP: application to precise determination of Rb, Sr, Y, Cs, Ba, REE, Pb, Th and U at ng g^{-1} level in milligram silicate samples. *Geostandards Newsletter* **21**, 307–319.

Makishima, A., Nakamura, E. & Nakano, T. (1997). Determination of boron in silicate samples by direct aspiration of sample HF solutions into ICP-MS. *Analytical Chemistry* **69**, 3754–3759.

Makishima, A., Nakamura, E. & Nakano, T. (1998). Determination of zirconium, niobium, hafnium and tantalum at ng g^{-1} levels in geological materials by direct nebulation of sample HF solutions into Fl-ICP-MS. *Geostandards Newsletter* **23**, 7–20.

Marsh, J. S., Hooper, P. R., Rehacek, J., Duncan, R. A. & Duncan, A. R. (1997). Stratigraphy and age of Karoo basalts of Lesotho and implications for correlations within the Karoo igneous province. In: Mahoney, J. J. & Coffin, M. F. (eds) *The Large Igneous Provinces: Continental, Oceanic, and Planetary Flood Volcanism. Geophysical Monograph, American Geophysical Union* **100**, 247–272.

Martin, A., Nisbet, E. G., Bickle, M. J. & Orpen, J. L. (1993). Rock units and stratigraphy of the Belingwe Greenstone Belt: the complexity of the tectonic setting. In: Bickle, M. J. & Nisbet, E. G. (eds) *The Geology of the Belingwe Greenstone Belt, Zimbabwe: a Study of Archean Continental Crust. Geological Society of Zimbabwe, Special Publication* **2**, 13–37.

Martin, H. (1986). Effect of steeper Archean geothermal gradient on geochemistry of subduction-zone magmas. *Geology* **14**, 753–756.

Martin, H. (1987). Petrogenesis of Archaean trondhjemites, tonalites and granodiorites from Eastern Finland: major and trace element geochemistry. *Journal of Petrology* **28**, 921–953.

Martin, H., Chauvel, C. & Jahn, B. M. (1983). Major and trace element geochemistry and crustal evolution of Archaean granodioritic rocks from eastern Finland. *Journal of Petrology* **21**, 159–180.

McDonough, W. F. & Ireland, T. R. (1993). Intraplate origin of komatiites inferred from trace elements in glass inclusions. *Nature* **365**, 432–434.

McDonough, W. F. & Sun, S.-S. (1995). The composition of the Earth. *Chemical Geology* **120**, 223–253.

Nakamura, E. & Kushiro, I. (1998). Trace element diffusion in jadeite and diopside melts at high pressures and its geochemical implication. *Geochimica et Cosmochimica Acta* **62**, 3151–3160.

Nakamura, E., Makishima, A., Moriguchi, T., Kobayashi, K., Sakaguchi, C., Yokoyama, T., Tanaka, R., Kuritani, T. & Takei, H. (2003). Comprehensive geochemical analyses of small amounts (<100 mg) of extraterrestrial samples for the analytical competition related to the sample-return mission, MUSES-C. *Institute of Space and Astronautical Science Report* **SP 16**, 49–101.

Nelson, D. R. (1998). Granite–greenstone crust formation on the Archean Earth: a consequence of two superimposed processes. *Earth and Planetary Science Letters* **158**, 109–119.

Nisbet, E. G., Arndt, N. T., Bickle, M. J., Cameron, W. E., Chauvel, C., Cheadle, M., Hegner, E., Kyser, T. K., Martin, A., Renner, R. & Roedder, E. (1987). Uniquely fresh 2·7 Ga komatiites from the Belingwe greenstone belt, Zimbabwe. *Geology* **15**, 1147–1150.

Nisbet, E. G., Bickle, M. J. & Martin, A. (1977). The mafic and ultramafic lavas of the Belingwe greenstone belt, Rhodesia. *Journal of Petrology* **18**, 521–566.

Nisbet, E. G., Cheadle, M. J., Arndt, N. T. & Bickle, M. J. (1993*a*). Constraining the potential temperature of the Archaean mantle: a review of the evidence from komatiites. *Lithos* **30**, 291–307.

Nisbet, E. G., Martin, A., Bickle, M. J. & Orpen, J. L. (1993*b*). The Ngezi Group: komatiites, basalts, and stromatolites on continental crust. In: Bickle, M. J. & Nisbet, E. G. (eds) *The Geology of the Belingwe Greenstone Belt, Zimbabwe*. Rotterdam: Balkema, pp. 121–165.

Parman, S. W., Dann, J. C., Grove, T. L. & de Wit, M. J. (1997). Emplacement conditions of komatiite magmas from the 3·49 Ga Komati Formation, Barberton Greenstone Belt, South Africa. *Earth and Planetary Science Letters* **150**, 303–323.

Parman, S. W., Shimizu, N., Grove, T. L. & Dann, J. C. (2003). Constraints on the pre-metamorphic trace element composition of Barberton komatiites from ion probe analyses of preserved clinopyroxene. *Contributions to Mineralogy and Petrology* **144**, 383–396.

Prendergast, M. D. (2004). The Bulawayan Supergroup: a late Archaean passive margin-related large igneous province in the Zimbabwe craton. *Journal of the Geological Society, London* **161**, 431–445.

Redman, B. A. & Keays, R. R. (1985). Archaean basic volcanism in the Eastern Goldfields Province, Yilgarn Block, Western Australia. *Precambrian Research* **30**, 113–152.

Renner, R., Nisbet, E. G., Cheadle, M. J., Arndt, N. T., Bickle, M. J. & Cameron, W. E. (1994). Komatiite flows from the Reliance Formation, Belingwe Belt, Zimbabwe: I. Petrography and mineralogy. *Journal of Petrology* **35**, 361–400.

Rudnick, R. L., McDonough, W. F., McCulloch, M. T. & Taylor, S. R. (1986). Lower crustal xenoliths from Queenland, Australia: evidence for deep crustal assimilation and fractionation. *Geochimica et Cosmochimica Acta* **50**, 1099–1115.

Sensarma, S., Palme, H. & Mukhopadhyay, D. (2002). Crust–mantle interaction in the genesis of siliceous high magnesian basalts: evidence from the Early Proterozoic Dongargarh Supergroup, India. *Chemical Geology* **187**, 21–37.

Shimizu, K., Komiya, T., Hirose, K., Shimizu, N. & Maruyama, S. (2001). Cr-spinel, an excellent micro-container for retaining primitive melts—implications for a hydrous plume origin for komatiites. *Earth and Planetary Science Letters* **189**, 177–188.

Shimizu, K., Nakamura, E., Kobayashi, K. & Maruyama, S. (2004). Discovery of Archean continental and mantle fragments inferred from xenocrysts in komatiites, the Belingwe greenstone belt, Zimbabwe. *Geology* **32**, 285–288.

Silva, K. E., Cheadle, M. J. & Nisbet, E. G. (1997). The origin of B1 zones in komatiite flows. *Journal of Petrology* **38**, 1565–1584.

Smithies, R. H. (2002). Archaean boninite-like rocks in an intracratonic setting. *Earth and Planetary Science Letters* **2002**, 19–34.

Smithies, R. H., Champion, C. D. & Sun, S.-S. (2004). Evidence for early LREE-enriched mantle source regions: diverse magmas from the *c.* 3·0 Ga Mallina Basin, Pilbara Craton, NW Australia. *Journal of Petrology* **45**, 1515–1537.

Stein, M. & Hofmann, A. W. (1994). Mantle plumes and episodic crustal growth. *Nature* **372**, 63–68.

Sylvester, P. J., Harper, G. D., Byerly, G. R. & Thurston, P. C. (1997). Volcanic aspects. In: de Wit, M. J. & Ashwal, L. D. (eds) *Greenstone Belts*. Oxford: Oxford University Press, pp. 55–90.

Takahashi, E. & Kushiro, I. (1983). Melting of a dry peridotite at high pressures and basalt magma genesis. *American Mineralogist* **68**, 859–879.

Takei, H. (2002). Development of precise analytical techniques for major and trace element concentrations in rock samples and their applications to the Hishikari Gold Mine, southern Kyushu, Japan. Doctoral thesis, Okamaya University.

Tanaka, R., Makishima, A., Kitagawa, H. & Nakamura, E. (2003). Suppression of Zr, Nb, Hf and Ta coprecipitation in fluoride compounds for determination in Ca-rich materials. *Journal of Analytical Atomic Spectrometry* **18**, 1458–1463.

Taylor, P. N., Kramers, J. D., Moorbath, S., Wilson, J. F., Orpen, J. L. & Martin, A. (1991). Pb/Pb, Sm–Nd and Rb–Sr geochronology in the Archean craton of Zimbabwe. *Chemical Geology (Isotope Geoscience Section)* **87**, 175–196.

Taylor, S. R. & McLennan, S. M. (1995). The geochemical evolution of the continental crust. *Reviews of Geophysics* **33**, 241–265.

Yokoyama, T., Makishima, A. & Nakamura, E. (1999). Evaluation of the coprecipitation of incompatible trace elements with fluoride during silicate rock dissolution by acid digestion. *Chemical Geology* **157**, 175–187.

Yoshikawa, M. & Nakamura, E. (2000). Geochemical evolution of the Horoman peridotite complex: implications for melt extraction, metasomatism and compositional layering in the mantle. *Journal of Geophysical Research* **105**, 2879–2901.

APPENDIX: ASSIMILATION–FRACTIONAL CRYSTALLIZATION (AFC) MODEL

AFC trends from the primary komatiite are calculated using a program written in C specifically for this purpose. The AFC model we used is a simple mass-balance calculation using seven major element abundances (i.e. SiO_2, TiO_2, Al_2O_3, FeO, MgO, CaO and $Na_2O + K_2O$; normalized to 100 wt %) in the primary komatiite, average komatiitic basalt and E-basalt (Table 4). The program iteratively calculates equilibrium olivine and subtracts this olivine from the komatiite liquid, and assimilates a contaminant into the liquid at certain A/FC ratios (R). An R of zero equals olivine fractional crystallization shown in Fig. 11. The compositions of the contaminants and R values for komatiitic basalt or E-basalt are set as unknown parameters. When the compositional difference between the calculated AFC melts

and komatiitic basalt or E-basalt reach a minimum, the program outputs the results in terms of the composition of the contaminant, R values and degree of contamination.

To simplify the AFC model, the calculations include four major assumptions as follows.

(1) The olivine–melt Fe–Mg partition coefficient is fixed at 0·32 with the Fe^{3+} content of the melt set to 10% of the total Fe. The TiO_2, Al_2O_3 and $Na_2O + K_2O$ contents of equilibrium olivines are 0 wt %, but the CaO content correlates with the Fo value according to the formula $0{\cdot}9 - (0{\cdot}0074 \times \mathrm{Fo})$. This expression was derived using the composition of olivine from the Belingwe komatiites.

(2) Olivine is the only phase that participates in crystallization. This assumption may be reasonable for the high-MgO samples in this study. Based on the MELTS program of Ghiorso & Sack (1995) and using the composition of the estimated parental komatiite, pyroxenes do not crystallize until the MgO content of the melt decreases to 10 wt % at 5 kbar under anhydrous conditions.

(3) The primary komatiite is not contaminated.

(4) The degree of contamination cannot exceed that of crystallization ($R < 1$), because the heat lost as a result of contamination should be compensated by the heat released by crystallization.

The R values, degrees of assimilation and the major element compositions of the contaminants for the komatiitic basalt and the E-basalt are obtained as shown in Table 4. The parameters used were as follows: R values were changed from 0 to 0·8 in 0·1 steps and the fractionation increment was fixed at 0·1 wt %.

The trace element (Sr, Zr, Nb, La, Nd, Sm, Dy, Yb, Pb, Th, U) and isotope compositions (Pb, Nd, Sr) of the contaminants were then evaluated based on the calculated major element compositions using a similar AFC model approach. The trace element distribution coefficients between olivine and melt were based on the values of Green (1994).